Robust Time-Based Localization for Asynchronous Networks

Yiyin Wang, *Student Member, IEEE*, Xiaoli Ma, *Senior Member, IEEE*, and Geert Leus, *Senior Member, IEEE*

Abstract—Time-based localization approaches attract a lot of interest due to their high accuracy and potentially low cost for wireless sensor networks (WSNs). However, time-based localization is tightly coupled with clock synchronization. Thus, the reliability of timestamps in time-based localization becomes an important yet challenging task to deal with. In this paper, we propose robust time-based localization strategies to locate a target node with the help of anchors (nodes with known positions) in asynchronous networks. Two kinds of asynchronous networks are considered: one only with clock offsets, labeled quasi-synchronous networks, whereas the other with not only clock offsets but also clock skews, labeled fully asynchronous networks. A novel ranging protocol is developed for both networks, namely asymmetric trip ranging (ATR), to reduce the communication load and explore the broadcast property of WSNs. Regardless of the reliability of the timestamp report from the target node, closed-form least-squares (LS) estimators are derived to accurately estimate the target node position. As a result, we counter the uncertainties caused by the target node by ignoring the timestamps from this node. Furthermore, in order to simplify the estimator in fully asynchronous networks, localization and synchronization are decoupled. A simple yet efficient method is proposed to first *Calibrate the Clock Skews* of the anchors, and then *Estimate the Node Position* (CCS-ENP). Finally, Cramér-Rao bounds (CRBs) and simulation results corroborate the efficiency of our localization schemes.

Index Terms—Clock offset, clock skew, least-squares, localization, synchronization, two-way ranging.

I. INTRODUCTION

D UE to their wide range of applications, such as target tracking, surveillance, environment monitoring, geographical routing and smart home, location-aware wireless sensor networks (WSNs) [1] have been intensively investigated [2]–[5]. Location-awareness is crucial for WSNs [4], [5]. To obtain accurate location estimates, range-based localization algorithms are more favorable than range-free ones [6]–[8]. In general, the range-based algorithms follow two steps [3]–[5]:

they first measure some metrics bearing location information, the so-called ranging or bearing, and second estimate the positions based on those metrics, the so-called location information fusion. There are mainly four metrics: time-of-arrival (TOA) or time-of-flight (TOF) [9], time-difference-of-arrival (TDOA) [10], [11], angle-of-arrival (AOA) [12], and received signal strength (RSS) [13]. The ranging methods using RSS can be implemented by energy detectors, but they can only achieve a coarse resolution. Antenna arrays are required for AOA-based methods, which encumbers their popularity. On the other hand, high accuracy and potentially low cost implementation make TOA or TDOA based on ultra-wideband impulse radios (UWB-IRs) a promising ranging method [4].

Since TOA or TDOA measurements are time-based, clock synchronization is essential to achieve accurate localization. Clock synchronization alone plays a critical role to guarantee general operations of WSNs. It is under intensive investigation [14]–[17] and results in various protocols, such as the Reference Broadcast Synchronization (RBS) protocol [18], the Timing-sync Protocol for Sensor Networks (TPSN) [19], and the Flooding Time Synchronization Protocol (FTSP) [20]. On the other hand, clock synchronization can also be handled by signal processing tools: a maximum likelihood estimator (MLE) for the clock offset is designed in [21], whereas theoretical performance limits for clock synchronization and MLEs for the clock offset and skew under different delay models, are developed in [22] and [23].

Because of the stringent cost and power constraints of WSNs, low-cost clocks are normally employed. This makes time-based localization and synchronization tightly coupled and challenging [17]. However, only recently the two entangled problems are jointly considered. A time-based positioning scheme (TPS) is developed in [24], where only the clock offset is considered. In [25], location in time and space is proposed, but only at the MAC and application layers. The two-way ranging (TWR) protocol proposed in the IEEE 802.15.4a standard [26] is employed in [27] for asynchronous networks. The relative clock skews are first calibrated, and then the node positions are estimated by a distributed maximum log-likelihood estimator (MLLE). Furthermore, a localization approach based on triple-differences, which are the differences of two differential TDOAs, is proposed in [28], where the corrupted one-way TOA measurements due to the relative clock offset and clock skew are corrected by several steps. The TWR protocol is also employed in [29], which considers TOA-based localization using practical clocks with internal delays and clock skews. Only recently, the joint estimation of the clock skew, the clock offset, and the position of the target node is proposed in [30]

for networks with synchronous anchors. A total least-squares (TLS) estimator is further proposed in [30] to take the uncertainties of the anchor positions and clock parameters into account. Moreover, the target node position and clock offset are estimated by a weighted least-squares (WLS) estimator in [31]. An asynchronous position measurement system is developed in [32] for indoor localization.

Due to the burgeoning of WSNs, localization is vulnerable to many types of attacks (see e.g., [33]–[35]). Lazos and Poovendran [36] propose Secure Range-independent Localization (SeRLoc) methods by taking advantage of antenna sectors in the presence of malicious adversaries. Capkun *et al.* [37] design Secure Positioning In sensor NEtworks (SPINE), which deal with distance modification attacks. Moreover, Chen *et al.* [38] design several attack detection schemes for wireless localization systems. Li *et al.* [39] propose to use least median squares (LMS) as the metric to develop localization algorithms, which tolerate outliers. Liu *et al.* [40] use the minimum mean square error (MMSE) as an indicator to filter out outliers, and further propose another method to bear with outliers by adopting an iteratively refined voting scheme.

In this paper, we consider time-related attacks which tightly connect with localization and synchronization. UWB-IRs are employed for high resolution TOA ranging [4], [41]. Low duty cycle, low probability of detection and speed of light transmission make UWB-IRs ideal for secure communication and localization. The TWR protocol in the IEEE 802.15.4a standard [26] promotes UWB ranging. However, this TWR protocol is vulnerable to an internal ranging attack by deceitful target nodes, which means that target nodes can send fraudulent timestamps to spoof their processing time. Furthermore, target nodes may submit inaccurate timestamps due to their asynchronous clocks or other reasons. Thus, the current protocol is not efficient and can even fail under the above circumstances.

We adopt UWB transmissions and propose robust TOA-based localization methods for asynchronous networks with possible internal attacks. We deal with two kinds of asynchronous networks: one with only clock offsets referred to as quasi-synchronous networks, whereas the other with not only clock offsets but also clock skews referred to as fully asynchronous networks. A novel ranging protocol, namely the asymmetric trip ranging (ATR) protocol is proposed in this paper by taking advantage of the broadcast property of WSNs. All the anchors can obtain ranging information in one ranging procedure. The ATR protocol reduces the communication load dramatically compared to the TWR protocol. In addition, by ignoring the processing time report from the target node, we estimate the target node position based only on the reliable timestamps from the anchors. As a result, the fact that the target node is not synchronized to the anchors, or an internal attack is mounted by a compromised target node, does not have any influence on the performance of our method. Furthermore, closed-form least-squares (LS) and WLS estimators are proposed for quasi-synchronous networks. For fully asynchronous networks, closed-form LS estimators are derived to jointly estimate the target position and clock parameters taking practical issues into account. To further simplify these estimators, synchronization and localization can be decoupled with almost no cost

in performance. A simple yet efficient solution is proposed to first **C**alibrate the **C**lock **S**kews of the anchors and then **E**stimate the **N**ode **P**osition (CCS-ENP). At the same time, our scheme is immune to an internal ranging attack. To the best of our knowledge, this is the first paper that combines all three aspects: localization, synchronization and security.

The rest of the paper is organized as follows. In Section II, we review the TWR protocol, analyze its error sources and explain its vulnerability. The robust time-based localization algorithms for quasi-synchronous and fully asynchronous networks are proposed in Sections III and IV, respectively. Performance bounds and simulation results are shown in Section V. The conclusions are drawn at the end of this paper.

Notation: We use upper (lower) bold face letters to denote matrices (column vectors). $[\mathbf{X}]_{m,n}$, $[\mathbf{X}]_{m,:}$ and $[\mathbf{X}]_{:,n}$ denote the element on the mth row and nth column, the mth row, and the nth column of the matrix $\mathbf{X}$, respectively. $[\mathbf{x}]_n$ indicates the nth element of $\mathbf{x}$. $\mathbf{0}_m$ ($\mathbf{1}_m$) and $\mathbf{I}_m$ are an all-zero (all-one) column vector of length m and an identity matrix of size $m \times m$, respectively. Moreover, $(\cdot)^T$, $\odot$, $|\cdot|$ and $\|\cdot\|$ designate transposition, element-wise multiplication, absolute value and ℓ_2 norm, respectively.

II. THE TWO-WAY RANGING PROTOCOL

The TWR protocol used in the IEEE 802.15.4a standard [26] facilitates ranging between two nodes. The packet structure proposed by the standard is composed of a synchronization header (SHR) preamble, a physical layer header (PHR) and a data field (see Fig. 3). The first pulse of the PHR is called the ranging marker (RMARKER). The moment when the RMARKER leaves or arrives at the antenna of a node is critical to ranging. An example of the TWR protocol is shown in Fig. 1. Node A (or Node B) records T_{AT} (or T_{BT}) and T_{AR} (or T_{BR}) upon the departure and the arrival of the RMARKER, respectively. Thus, the time of flight (TOF) t_0, which is linear to the distance d (the ranging target) between node A and node B ($d = ct_0$, where c is the speed of light), is given by

$$t_0 = \frac{1}{2}\left(\frac{T_{AR} - T_{AT}}{\alpha_A} - \frac{\tau_0}{\alpha_B}\right) + n \qquad (1)$$

where $\tau_0 = T_{BT} - T_{BR}$ is the processing time at node B, α_A and α_B are the clock skews of node A and node B, respectively, and n is the aggregate error term. In general, τ_0 is several hundreds of milliseconds and t_0 is several tens of nanoseconds for an indoor environment. As a result, τ_0 is heavily influenced by clock drift due to the relative clock skew between node A and node B.

As the differences of the timestamps are employed in (1), the clock offsets are canceled. The aggregate error term n in (1) accounts for different kinds of errors, such as the leading edge detection (LED) errors [26], [42], and the uncertainties of the internal delays [26], [29], which we explain next. The LED errors are due to the detection of the first multipath component of the received RMARKER. It is not a trivial task to detect the first multipath component, or in other words, the leading edge of the first cluster of the arriving RMARKER. It depends on the multipath channel, the signal bandwidth, the signal-to-noise ratio (SNR) and the detection strategy [4]. Even if we can detect the
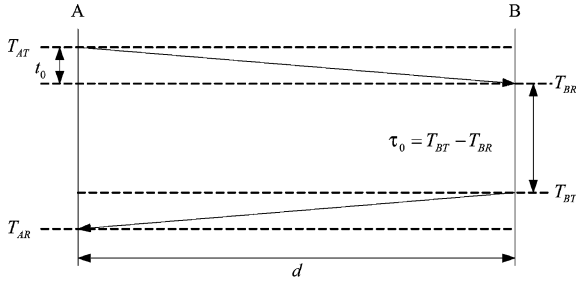
Fig. 1. An example of the TWR protocol.

leading edge accurately, there may still be a ranging bias due to different kinds of environments. The LED could lead to accurate ranging for line-of-sight (LOS). However, the TOF of the first arriving multipath component in non-line-of-sight (NLOS) environments may not indicate the correct distance information due to the obstacles between two ranging nodes. In that case, the TOF estimates are biased, and calibration is indispensable to remove the bias. A ranging model that can distinguish between different environments is proposed in [42]. A more sophisticated ranging model as an enhancement of [42] is presented in [27], which takes the detection noise and the drift compensation into account. Next to LED errors, internal delays are caused by the difficulty to measure events at the antenna exactly. Since the ranging counter is typically somewhere in the digital section, the signal has to go through some transmitting (or receiving) chain after (or before) the ranging counter records the timestamp to reach the antenna (or the ranging counter). There is a difference between the real time the RMARKER leaves or arrives at the antenna and the recorded time by the ranging counter. This time-varying internal delay can be a few hundreds of nanoseconds depending on the transceiver structure [29]. The standard proposes a calibration mechanism to compensate for the internal propagation time but some uncertainties still remain. Note that n can also contain communication and quantization errors as discussed next. Since the timestamps are distributed over the two nodes, they have to be brought together, which cannot be accomplished perfectly due to the limited communication resources. Furthermore, the abstract ranging counter, which assigns values to the timestamps, runs at a nominal 64 GHz in the standard, which causes some quantization effects.

We remark that the timestamps employed for ranging are different from the timestamps used in traditional clock synchronization protocols. Since the timestamps used here are recorded at the physical layer when the RMARKER leaves or arrives at the antenna, it excludes most of the conventional sources of uncertainty of message delivery delays in clock synchronization [19], [20], [43], including send time, access time, reception time and receive time, which are the main error sources in clock synchronization. The TOF for ranging, called the propagation time in clock synchronization, is one of the sources of uncertainty of message delivery delays, but it only contributes a little compared to other sources in traditional clock synchronization. Therefore, if these timestamps are used not only for ranging, but also for clock synchronization, a much better accuracy could be achieved than the existing clock synchronization protocols (see

[14], [19], [20], and references therein). This kind of physical layer synchronization is also referred to as the pulse coupling method in [15].

Let us now focus on the security issues of the TWR protocol. The standard provides optional private ranging as a secure mode. The dynamic preamble selection and the encryption of the timestamp reports are used to facilitate the private ranging [26], [41]. However, the TWR protocol is vulnerable to an internal attack, which cannot be addressed by conventional cryptographic countermeasures. According to (1), the TOF t_0 depends not only on the timestamps T_{AR} and T_{AT} at node A, but also on the processing time τ_0 at node B. The dependence on the reliability and synchronization of two different nodes is a weak point of the TWR protocol. For example, assume node B is compromised and tries to cheat node A about its distance by tampering its processing time as τ_0'. Then, t_0 will be miscalculated, since node A is not aware of the attack. In the following, we adopt the same signal structure as in Fig. 3 and propose a new protocol which is immune to internal attacks.

III. LOCALIZATION FOR QUASI-SYNCHRONOUS NETWORKS

Considering M anchor nodes and one target node, we would like to estimate the position of the target node. All the nodes are distributed in an l-dimensional space, e.g., $l = 2$ (a plane) or $l = 3$ (a space). The coordinates of the anchor nodes are known and defined as $\mathbf{X}_a = [\mathbf{x}_1, \mathbf{x}_2, \ldots, \mathbf{x}_M]_{l \times M}$, where the vector $\mathbf{x}_i = [x_{1,i}, x_{2,i}, \ldots, x_{l,i}]^T$ of length l indicates the known coordinates of the ith anchor node. We employ a vector $\mathbf{x}$ of length l to denote the unknown coordinates of the target node. Our method can also be extended for multiple target nodes. We remark that in a large scale WSN, it is common to localize target nodes in a sequential way [19], [30]. The target nodes that have enough anchors are localized first. Then, these located target nodes can be viewed as new anchors that can facilitate the localization of other target nodes. Therefore, the scenario here is of practical interest. In this section, we tackle quasi-synchronous networks, and we leave the fully asynchronous case to the next section.

A. System Model

In quasi-synchronous networks, the target node clock runs freely, and the clock skews of all the anchors are equal to 1 or treated as 1. There are only clock offsets among all the anchors. The timing relation between the ith anchor clock $C_i(t)$ and the absolute time t can be described as [14]

$$C_i(t) = t + \theta_i, \quad i = 1, 2, \ldots, M, \tag{2}$$

where θ_i is the unknown clock offset of $C_i(t)$ relative to the absolute clock. Moreover, the model for the target clock is given by

$$C_s(t) = \alpha_s t + \theta_s, \tag{3}$$

where α_s and θ_s denote the unknown clock skew and clock offset of the target node clock relative to the absolute clock.

A novel asymmetric trip ranging (ATR) protocol is shown in Fig. 2, which subsumes the protocol used in [44] as a special
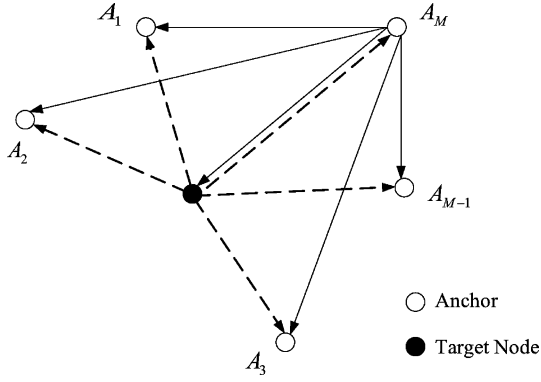
Fig. 2. An illustration of the ATR protocol.

case. The ATR protocol makes all the other anchors listen to the ranging packets and record timestamps locally, when one anchor and the target node exchange their ranging packets. It can obtain more information than the TWR protocol, where all the other nodes are idle, when two nodes exchange their ranging packets. The ATR protocol starts with one of the anchors initiating the ranging request and recording a timestamp when its RMARKER departs, which can also be interpreted as the time when that anchor receives its own RMARKER without any delay. Without loss of generality, we assume the Mth anchor initiates the ranging request, and we denote the time recorded at the Mth anchor as T_{MR}. Consequently, all the other anchors and the target node receive the ranging request and record their own timestamps $T_{iR}, i = 1, 2, \ldots, M - 1$ and T_{SR}, respectively, as soon as they detect the RMARKER from the Mth anchor. The target node processes the ranging request and broadcasts a response. The departure time of the target RMARKER is recorded as T_{ST}, and we define $\tau = T_{ST} - T_{SR}$ as the true processing time of the target node. Each anchor in the network detects the broadcasted ranging response from the target node, and records its own timestamp for the arrival of the target RMARKER as $T_{iS}, i = 1, 2, \ldots, M$. If a compromised target node tampers its processing time as τ', or a target node reports τ' due to the clock skew or the internal delay, all the distance measurements would be decreased or enlarged by $c|\tau - \tau'|$ (where c is the speed of light), which would lead to a meaningless position estimate.

For the ith anchor node, the difference between T_{iS} and T_{iR} relates to the distance as

$$c(T_{iS} - T_{iR}) = d_i + d_M + \Delta - d_{iM} + n_{iS} - n_{iR}$$
$$i = 1, 2, \ldots, M \quad (4)$$

where $d_i = \|\mathbf{x}_i - \mathbf{x}\| = \sqrt{\|\mathbf{x}_i\|^2 - 2\mathbf{x}_i^T \mathbf{x} + \|\mathbf{x}\|^2}$ is the unknown distance between the ith anchor and the target node, $\Delta = c\tau$ is the unknown distance corresponding to the target node processing time, and $d_{iM} = \|\mathbf{x}_i - \mathbf{x}_M\|$ is the known distance between the ith and the Mth anchors. Furthermore, n_{iS} and n_{iR} denote the distance errors translated from the measurement errors of T_{iS} and T_{iR}, respectively, which are aggregate error terms, as we have discussed in Section II. Note that the recordings of T_{iS} and $T_{iR}, i = 1, 2, \ldots, M - 1$ are triggered by the received RMARKERs, and thus the same internal delays are involved, which are canceled out by making differences of

timestamps recorded at the same node as indicated in (4). By making these differences, the clock offsets at the anchors are canceled as well.[1] The situation is different for the Mth anchor, since it records T_{MR} and T_{MS} upon transmitting and receiving the RMARKERs, respectively. As a result, the internal delays of the transmission path and the receiving path are added up when computing $T_{MS} - T_{MR}$. Thus, we assume that the main part of the Mth anchor's internal delay is compensated beforehand as accomplished in [29]. But different from [29], compensation is not required for the other anchors in our scheme. Consequentially, n_{iS} and n_{iR} can be modeled as zero-mean random variables with variance σ_{iS}^2 and σ_{iR}^2, respectively [42]. Note that the timestamps employed here are recorded at the physical layer, which are totally different from the conventional timestamps recorded at the MAC or other upper layers in clock synchronization, which have different error sources. A NLOS environment would introduce a biased LED error, and in that case n_{iS} or n_{iR} will have a non-zero mean. However, since this bias is not known, the only safe assumption is to view it as zero mean, or we assume that a calibration is carried out to remove it beforehand. More sophisticated error models such as the one in [27] can be considered in future work. Defining $\mathbf{u} = c[T_{1S}, T_{2S}, \ldots, T_{MS}]^T$, $\mathbf{v} = c[T_{1R}, T_{2R}, \ldots, T_{MR}]^T$, $\mathbf{d} = [d_1, d_2, \ldots, d_M]^T$, $\mathbf{d}_a = [d_{1M}, d_{2M}, \ldots, d_{(M-1)M}, 0]^T$, $\mathbf{n}_s = [n_{1S}, n_{2S}, \ldots, n_{MS}]^T$ and $\mathbf{n}_r = [n_{1R}, n_{2R}, \ldots, n_{MR}]^T$, we can write (4) in vector form as

$$\mathbf{u} - \mathbf{v} = \mathbf{d} + (d_M + \Delta)\mathbf{1}_M - \mathbf{d}_a + \mathbf{n}_s - \mathbf{n}_r. \quad (5)$$

In order to be immune to an internal attack by the compromised target node or to incorrect timestamps due to the randomness of the target node clock, we do not employ the timestamp report from the target node, but only use it as a trigger at each anchor. We estimate the target position only based on the timestamps T_{iR} and $T_{iS}, i = 1, 2, \ldots, M$, recorded locally at the M anchors. Because we do not use the timestamps of the target node, its clock parameters, such as clock skew, clock offset and internal delay, do not have any impact on our scheme. This distinguishes our algorithm from others that use the timestamps of the target node, such as [27], [29], [30]. It is easy for the target node to cheat one anchor, but it is almost impossible to cheat all the anchors simultaneously. We remark that the cooperative positioning protocol proposed in [45] is similar to our ATR protocol. However, our method differs from [45] in several aspects: (i) we do not use the timestamps from the target node, and thus our method is more robust to unreliable timestamps; (ii) the target node processing time is unknown; and (iii) we propose low-complexity closed-form solutions for localization, instead of complex MLEs.

B. Localization Algorithm

Since we do not use the timestamps from the target node, the clock parameters of the target node do not impact its position estimate. More specifically, we treat Δ (the distance corresponding to the target node processing time) in (5) as an unknown parameter. Note that (5) is a linear equation with respect

---

[1]Note that this is different from the traditional TDOA approach, which requires synchronization among anchor nodes [5].

to (w.r.t.) Δ, but it is a complicated nonlinear equation w.r.t. $\mathbf{x}$ due to d_M and $\mathbf{d}$. We are not interested in methods with a high computational complexity, such as the MLE which also requires the unknown noise pdf. Because of the low-cost and low-power constraints of a WSN, we explore low-complexity closed-form solutions for localization.

Since $\Delta \gg d_i$, Δ is a dominant term at the right hand side of (5). In order to extract useful distance information, we have to preprocess (5). Instead of choosing a reference anchor node as proposed in [44], we employ an orthogonal projection $\mathbf{P}$ onto the orthogonal complement of $\mathbf{1}_M$, which is given by $\mathbf{P} = \mathbf{I}_M - \frac{1}{M}\mathbf{1}_M\mathbf{1}_M^T$. Since $\mathbf{P}\mathbf{1}_M = \mathbf{0}_M$, $\mathbf{P}$ can be used to eliminate the term $(d_M + \Delta)\mathbf{1}_M$ in (5). As a result, premultiplying both sides of (5) with $\mathbf{P}$, we obtain

$$\mathbf{P}(\mathbf{u} - \mathbf{v}) = \mathbf{P}\mathbf{d} - \mathbf{P}\mathbf{d}_a + \mathbf{P}(\mathbf{n}_s - \mathbf{n}_r). \quad (6)$$

Note that $\mathbf{P}\mathbf{d} = \mathbf{d} - \bar{d}\mathbf{1}_M$, where $\bar{d} = \frac{1}{M}\sum_{i=1}^M d_i$ is the unknown average of the distances between the target node and the anchors. Thus, (6) can be rewritten as

$$\mathbf{P}(\mathbf{u} - \mathbf{v}) = \mathbf{d} - \bar{d}\mathbf{1}_M - \mathbf{P}\mathbf{d}_a + \mathbf{P}\mathbf{n}_s - \mathbf{P}\mathbf{n}_r. \quad (7)$$

Keeping $\mathbf{d}$ on one side, moving the other terms to the other side, and making an element-wise multiplication, we achieve

$$\begin{aligned}
\boldsymbol{\psi}_a - &2\mathbf{X}_a^T\mathbf{x} + \|\mathbf{x}\|^2\mathbf{1}_M \\
&= (\mathbf{P}(\mathbf{u} - \mathbf{v} + \mathbf{d}_a)) \odot (\mathbf{P}(\mathbf{u} - \mathbf{v} + \mathbf{d}_a)) + \bar{d}^2\mathbf{1}_M \\
&+ 2\bar{d}\mathbf{P}(\mathbf{u} - \mathbf{v} + \mathbf{d}_a) + \mathbf{n}_{rs},
\end{aligned} \quad (8)$$

where $\boldsymbol{\psi}_a = [\|\mathbf{x}_1\|^2, \|\mathbf{x}_2\|^2, \dots, \|\mathbf{x}_M\|^2]^T$, and

$$\begin{aligned}
\mathbf{n}_{rs} &= (\mathbf{P}(\mathbf{n}_r - \mathbf{n}_s)) \odot (\mathbf{P}(2(\mathbf{u} - \mathbf{v} + \mathbf{d}_a) + \mathbf{n}_r - \mathbf{n}_s)) \\
&+ 2\bar{d}\mathbf{P}(\mathbf{n}_r - \mathbf{n}_s), \\
&= -(\mathbf{P}(\mathbf{n}_s - \mathbf{n}_r)) \odot (\mathbf{P}(\mathbf{n}_s - \mathbf{n}_r)) - 2\mathbf{d} \odot \mathbf{P}(\mathbf{n}_s - \mathbf{n}_r).
\end{aligned} \quad (9)$$

Defining $\mathbf{P}\mathbf{n}_r = \mathbf{n}_r - \bar{n}_r\mathbf{1}_M$ and $\mathbf{P}\mathbf{n}_s = \mathbf{n}_s - \bar{n}_s\mathbf{1}_M$, where $\bar{n}_r = \frac{1}{M}\sum_{i=1}^M n_{iR}$ and $\bar{n}_s = \frac{1}{M}\sum_{i=1}^M n_{iS}$, we can write the entries of $\mathbf{n}_{rs}$ as

$$\begin{aligned}
[\mathbf{n}_{rs}]_i &= 2d_i(n_{iR} - \bar{n}_r - n_{iS} + \bar{n}_s) \\
&- (n_{iR} - \bar{n}_r - n_{iS} + \bar{n}_s)^2, \quad i = 1, 2, \dots, M. \quad (10)
\end{aligned}$$

Recall that $E[n_{iS}] = 0$, $E[n_{iS}^2] = \sigma_{iS}^2$ and $E[n_{iS}n_{jS}] = 0$, $i \neq j$, leading to $E[\bar{n}_s] = 0$, $E[\bar{n}_s^2] = \frac{1}{M^2}\sum_{i=1}^M \sigma_{iS}^2$ and $E[\bar{n}_s n_{iS}] = \frac{1}{M}\sigma_{iS}^2$. The stochastic properties of n_{iR} can be obtained in a similar way. Moreover, n_{iS} and $n_{iR}, i = 1, 2, \dots, M$ are uncorrelated. As a result, the stochastic properties of $\mathbf{n}_{rs}$ are given by

$$E[[\mathbf{n}_{rs}]_i] = \frac{2 - M}{M}(\sigma_{iR}^2 + \sigma_{iS}^2) - \frac{1}{M^2}\sum_{k=1}^M(\sigma_{kR}^2 + \sigma_{kS}^2) \approx 0 \quad (11)$$

where we ignore the higher order noise terms to obtain (12), shown at the bottom of the page, and assume $E[[\mathbf{n}_{rs}]_i] \approx 0$ under the condition of sufficiently small measurement errors. Note that the noise covariance matrix $\boldsymbol{\Sigma}_{rs}$ depends on the unknown $\mathbf{d}$.

As (8) is still a nonlinear equation w.r.t. $\mathbf{x}$, we make again use of the orthogonal projection $\mathbf{P}$ to eliminate the terms $\|\mathbf{x}\|^2$ and $\bar{d}^2$ in (8). By premultiplying both sides of (8) with $\mathbf{P}$ and rearranging the terms, we arrive at

$$\begin{aligned}
\mathbf{P}\boldsymbol{\psi}_a - &\mathbf{P}((\mathbf{P}(\mathbf{u} - \mathbf{v} + \mathbf{d}_a)) \odot (\mathbf{P}(\mathbf{u} - \mathbf{v} + \mathbf{d}_a))) \\
&= 2\mathbf{P}\mathbf{X}_a^T\mathbf{x} + 2\bar{d}\mathbf{P}(\mathbf{u} - \mathbf{v} + \mathbf{d}_a) + \mathbf{P}\mathbf{n}_{rs}. \quad (13)
\end{aligned}$$

As a result, (13) becomes a linear equation w.r.t. both $\mathbf{x}$ and $\bar{d}$. Defining $\mathbf{b} = \boldsymbol{\psi}_a - ((\mathbf{P}(\mathbf{u} - \mathbf{v} + \mathbf{d}_a)) \odot (\mathbf{P}(\mathbf{u} - \mathbf{v} + \mathbf{d}_a)))$, $\mathbf{A} = 2[\mathbf{X}_a^T, \mathbf{P}(\mathbf{u} - \mathbf{v} + \mathbf{d}_a)]$, and $\mathbf{y} = [\mathbf{x}^T, \bar{d}]^T$, we can finally rewrite (13) as

$$\mathbf{P}\mathbf{b} = \mathbf{P}\mathbf{A}\mathbf{y} + \mathbf{P}\mathbf{n}_{rs}. \quad (14)$$

We can find the LS and WLS solutions for (14) as

$$\hat{\mathbf{y}} = (\mathbf{A}^T\mathbf{P}\mathbf{A})^{-1}\mathbf{A}^T\mathbf{P}\mathbf{b}, \quad (15)$$

and

$$\hat{\mathbf{y}} = (\mathbf{A}^T\mathbf{P}\mathbf{W}\mathbf{P}\mathbf{A})^{-1}\mathbf{A}^T\mathbf{P}\mathbf{W}\mathbf{P}\mathbf{b} \quad (16)$$

respectively, where $\mathbf{W}$ is a weighting matrix. The optimal weighting matrix $\mathbf{W}_o$ is given by

$$\mathbf{W}_o = (\mathbf{P}\boldsymbol{\Sigma}_{rs}\mathbf{P})^\dagger \quad (17)$$

where we use the pseudo inverse because the $M \times M$ projection matrix $\mathbf{P}$ has rank $M - 1$. Furthermore, $\mathbf{P}\mathbf{A}$ should be a full rank tall matrix. Thus, the number of anchors M should be no less

$$\begin{aligned}
[\boldsymbol{\Sigma}_{rs}]_{i,j} &= E[[\mathbf{n}_{rs}]_i[\mathbf{n}_{rs}]_j] \\
&= E[(2d_i(n_{iR} - \bar{n}_r - n_{iS} + \bar{n}_s) - (n_{iR} - \bar{n}_r - n_{iS} + \bar{n}_s)^2) \\
&\quad \times (2d_j(n_{jR} - \bar{n}_r - n_{jS} + \bar{n}_s) - (n_{jR} - \bar{n}_r - n_{jS} + \bar{n}_s)^2)] \\
&\approx 4d_id_jE[(n_{iR} - \bar{n}_r - n_{iS} + \bar{n}_s)(n_{jR} - \bar{n}_r - n_{jS} + \bar{n}_s)] \\
&\approx \begin{cases} 4d_i^2\left(\frac{M-2}{M}(\sigma_{iR}^2 + \sigma_{iS}^2) + \frac{1}{M^2}\sum_{k=1}^M(\sigma_{kR}^2 + \sigma_{kS}^2)\right), & i = j \\ 4d_id_j\left(\frac{1}{M^2}\sum_{k=1}^M(\sigma_{kS}^2 + \sigma_{kR}^2) - \frac{1}{M}(\sigma_{iS}^2 + \sigma_{jS}^2 + \sigma_{iR}^2 + \sigma_{jR}^2)\right), & i \neq j \end{cases}
\end{aligned} \quad (12)$$

than $l + 3$, which indicates that we need at least five anchors to estimate the target position on a plane. Since $\mathbf{W}_o$ depends on the unknown $\mathbf{d}$, we can update it iteratively. Consequently, the iterative WLS is summarized as follows:

1) Initialize $\mathbf{W}$ using the estimate of $\mathbf{d}$ based on the LS estimate of $\mathbf{x}$;
2) Estimate $\hat{\mathbf{y}}$ using (16);
3) Construct $\mathbf{W}$ using (17), where $\mathbf{\Sigma}_{rs}$ is computed using $\hat{\mathbf{y}}$;
4) Repeat Steps 2) and 3) until no obvious improvement of the cost function $(\mathbf{b} - \mathbf{A}\mathbf{y})^T \mathbf{P}\mathbf{W}\mathbf{P}(\mathbf{b} - \mathbf{A}\mathbf{y})$ is observed.

An estimate of $\mathbf{x}$ is finally given by

$$\hat{\mathbf{x}} = [\mathbf{I}_l \quad \mathbf{0}_l]\hat{\mathbf{y}}. \tag{18}$$

We remark that the estimator (15) [or (16)] is equivalent to the unconstrained LS (or WLS) estimator to obtain $\mathbf{x}, \bar{d}$ and $\bar{d}^2 - \|\mathbf{x}\|^2$ all together as discussed in [46]. We may even improve the estimation performance by exploring the relations among $\mathbf{x}$, $\bar{d}$ and $\bar{d}^2 - \|\mathbf{x}\|^2$ as constraints. Constrained LS (CLS) and weighted CLS estimators can be derived as in [9], [10]. However, it is extremely difficult to take the relation between $\mathbf{x}$ and $\bar{d}$ into account, since it is highly nonlinear.

The distance Δ corresponding to the target node processing time can be estimated as

$$\hat{\Delta} = \mathbf{1}_M^T(\mathbf{u} - \mathbf{v} - \hat{\mathbf{d}} + \mathbf{d}_a) - \hat{d}_M \tag{19}$$

where $\hat{d}_i = \|\hat{\mathbf{x}} - \mathbf{x}_i\|, i = 1, 2, \ldots, M$ are the distance estimates between the target node and the anchors based on $\hat{\mathbf{x}}$. We remark that there are mathematical similarities between our data model (5) and the data model in [29], if we regard $d_M + \Delta$ in (5) as an unknown internal delay. However, we employ a novel ATR protocol and estimate the parameters in a different way.

IV. LOCALIZATION FOR FULLY ASYNCHRONOUS NETWORKS

A. System Model

In this section, we release all the synchronization constraints on the anchors and the target node. There are not only clock offsets, but also clock skews among all the anchors and the target node. We use the same clock model (3) here for the target node to indicate its clock skew α_s and clock offset θ_s. The anchor clock model $C_i(t)$ is now given by

$$C_i(t) = \alpha_i t + \theta_i, i = 1, 2, \ldots, M \tag{20}$$

where α_i denotes the unknown clock skew of $C_i(t)$ relative to the absolute clock, and θ_i again is the unknown clock offset. Thus, the relations between the clocks $C_i(t)$ and $C_j(t)$ are given by

$$C_i(t) = \frac{\alpha_i}{\alpha_j}C_j(t) - \frac{\alpha_i}{\alpha_j}\theta_j + \theta_i. \tag{21}$$

Applying the same ATR protocol as in Section III-A, we obtain T_{iR} and $T_{iS}, i = 1, 2, \ldots, M$, which are in total $2M$ timestamps. Fig. 3 shows an example of a transmitted ranging packet and a received ranging packet. The time intervals in Fig. 3 are measured by the local clocks of the nodes. The length of the preamble is defined as T_p. Since the ranging packet is gener-
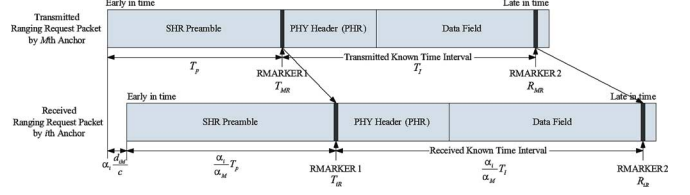

Fig. 3. An example of a transmitted ranging packet and a received ranging packet.

ated by the Mth anchor, it generates the preamble of length T_p relative to its own clock. The ith anchor regards the length of the received preamble as $\alpha_i T_p/\alpha_M$ due to the relative clock skew. Therefore, the difference between T_{iR} and T_{MR} is not only related to the TOF between the anchors (measured by the ith anchor as $\alpha_i d_{iM}/c$), but also to the relative clock drift over the whole preamble. However, the relations between the two timestamps recorded at the same anchor are relatively simple. By making differences of the timestamps from the same anchor, the clock offsets are again canceled out. As a result, the difference between T_{iS} and T_{iR} can be described as

$$\frac{c}{\alpha_i}(T_{iS} - T_{iR}) = d_i + d_M + \Delta - d_{iM}$$
$$+ \frac{n_{iS}}{\alpha_i} - \frac{n_{iR}}{\alpha_i}, \quad i = 1, 2, \ldots, M. \tag{22}$$

There is no impact of the relative clock drift over the whole preamble in (22). Note that the error terms n_{iS} and n_{iR} are also influenced by the clock skew of the ith anchor. We remark that the target clock does not have any impact on (22), but the influence of the asynchronous anchors remains. This again confirms that ignoring the timestamps from the target node can thwart internal attacks.

In (22), there are M equations and $M + l + 1$ unknown parameters in total. It is clear that there are not enough observation data (timestamps) to estimate all the parameters, if the ranging procedure is only executed once. To solve that problem, the ranging procedure can be repeated several times in order to obtain sufficient observations for making an accurate estimate as in [47]. However, in a power-hungry WSN, data communications could consume much more power than data processing [48], and the communication load should be reduced as much as possible. Therefore, we would like to add another RMARKER in the ranging packet to facilitate the clock synchronization in order to achieve the lowest communication load. The new ranging packet not only includes RMARKER1 in the PHY header (PHR), but also has another RMARKER2 as the first pulse in the last symbol of the data field as shown in Fig. 3. We further make use of the prior knowledge about the length of the ranging packet, and thus the time interval T_I between RMARKER1 and RMARKER2 is known to all the anchors. The length of the received ranging packet can be extended or reduced due to the relative clock skew of the receiver clock, and thus yields the parameter bearing the information of the relative clock skew. This parameter is different from the ones used in [29], [42], where ranging packets have to be consecutively or periodically transmitted. By making use of the known

length of the ranging packet [42] or the known transmission period [29], they also obtain parameters bearing the relative clock skew information. However, our scheme has a smaller communication load than theirs. In Fig. 3, we show an example of an extended ranging packet, where the clock skew difference between the receiver and the transmitter is positive. We remark that T_I should be long enough to observe sufficient clock drift, which means that after T_I the clock drift should be larger than the resolution of the TOA estimation. According to the standard, the time interval T_I could be several milliseconds, e.g., 5 ms. With a typical value of the relative clock skew of 40 ppm, we will observe 200 ns clock difference after 5 ms, whereas the resolution of TOA estimation using an UWB signal with a 1 GHz bandwidth can reach several nanoseconds [4]. Therefore, using a standard ranging packet, it is sufficient to estimate the drift between RMARKER1 and RMARKER2. Consequently, each anchor records two timestamps, when it receives a ranging packet during the procedure. The first set of timestamps is still represented by T_{iR} and T_{iS}, while the second one is denoted by R_{iR} and R_{iS}. Their relations are summarized as

$$\frac{c}{\alpha_i}(R_{iR} - T_{iR}) = \frac{cT_I}{\alpha_M} + \frac{m_{iR}}{\alpha_i} - \frac{n_{iR}}{\alpha_i}$$
$$i = 1, 2, \ldots, M \quad (23)$$

$$\frac{c}{\alpha_i}(R_{iS} - T_{iS}) = \frac{cT_I}{\alpha_s} + \frac{m_{iS}}{\alpha_i} - \frac{n_{iS}}{\alpha_i}$$
$$i = 1, 2, \ldots, M \quad (24)$$

where m_{iR} and m_{iS} are the corresponding distance errors due to the measurement errors of R_{iR} and R_{iS}, respectively. We assume that the variances of the measurement errors for RMARKER1 and RMARKER2 in the same packet are the same, and thus m_{iR} and m_{iS} are also modeled as zero-mean random variables with variances σ_{iR}^2 and σ_{iS}^2, respectively. Note that the clock skew of the target α_s in (24) influences the time differences between RMARKER1 and RMARKER2 of the ranging response, which are generated by the target node. We remark that the other clock parameters of the target node, i.e., the clock offset and the internal delay, do not influence our scheme, since we still do not use the timestamps from the target node.

We can now write (22), (23) and (24) in vector form as

$$\mathbf{F}_1 \boldsymbol{\gamma} = \frac{cT_I}{\alpha_M} \mathbf{1}_M + \text{diag}(\boldsymbol{\gamma})(\mathbf{m}_r - \mathbf{n}_r) \quad (25)$$

$$\mathbf{F}_2 \boldsymbol{\gamma} = \frac{cT_I}{\alpha_s} \mathbf{1}_M + \text{diag}(\boldsymbol{\gamma})(\mathbf{m}_s - \mathbf{n}_s) \quad (26)$$

$$\mathbf{F}_3 \boldsymbol{\gamma} = \mathbf{d} + (d_M + \Delta)\mathbf{1}_M - \mathbf{d}_a + \text{diag}(\boldsymbol{\gamma})(\mathbf{n}_s - \mathbf{n}_r) \quad (27)$$

where $\boldsymbol{\gamma} = [1/\alpha_1, 1/\alpha_2, \ldots, 1/\alpha_M]^T$, $\mathbf{F}_1 = \text{diag}(\mathbf{p} - \mathbf{v})$, $\mathbf{F}_2 = \text{diag}(\mathbf{q} - \mathbf{u})$, $\mathbf{F}_3 = \text{diag}(\mathbf{u} - \mathbf{v})$, $\mathbf{p} = c[R_{1R}, R_{2R}, \ldots, R_{MR}]^T$, $\mathbf{q} = c[R_{1S}, R_{2S}, \ldots, R_{MS}]^T$, $\mathbf{m}_r = [m_{1R}, m_{2R}, \ldots, m_{MR}]^T$, and $\mathbf{m}_s = [m_{1S}, m_{2S}, \ldots, m_{MS}]^T$. Recall that $\mathbf{u} = c[T_{1S}, T_{2S}, \ldots, T_{MS}]^T$ and $\mathbf{v} = c[T_{1R}, T_{2R}, \ldots, T_{MR}]^T$. Our goal is to estimate $\mathbf{x}$, $\boldsymbol{\gamma}$ and Δ based on (25)–(27). Note that the last equation in (25) does not offer any useful information, since $1/\alpha_M$ is at both sides of the equation. Thus,

we collect the $3M - 1$ equations related to $\boldsymbol{\gamma}$ and write them in vector form as

$$\mathbf{F}\boldsymbol{\gamma} = \begin{bmatrix} \mathbf{0}_{M-1} \\ \frac{1}{\alpha_s}cT_I\mathbf{1}_M \\ \mathbf{d} + (d_M + \Delta)\mathbf{1}_M - \mathbf{d}_a \end{bmatrix}$$
$$+ \begin{bmatrix} \mathbf{Z}\text{diag}(\boldsymbol{\gamma})(\mathbf{m}_r - \mathbf{n}_r) \\ \text{diag}(\boldsymbol{\gamma})(\mathbf{m}_s - \mathbf{n}_s) \\ \text{diag}(\boldsymbol{\gamma})(\mathbf{n}_s - \mathbf{n}_r) \end{bmatrix} \quad (28)$$

where

$$\mathbf{F} = [\mathbf{F}_1^T \mathbf{Z}^T - \mathbf{E}_1^T, \mathbf{F}_2^T, \mathbf{F}_3^T]^T$$
$$\mathbf{E}_1 = [\mathbf{0}_{(M-1)\times(M-1)}, cT_I\mathbf{1}_{M-1}]$$

and

$$\mathbf{Z} = [\mathbf{I}_{M-1}, \mathbf{0}_{M-1}].$$

B. Localization Algorithm

From now on, we ignore the error terms in the analysis for simplicity. The localization algorithms based on (25)–(27) are also naturally immune to the unreliable timestamps from the target node, and robust to the randomness of the target node clock, since we do not use the timestamps from the target node. We would like to investigate low-complexity localization methods. Although the data model (28) is a complicated nonlinear equation w.r.t. $\mathbf{x}$, it is linear w.r.t. to $\boldsymbol{\gamma}$. We can first estimate $\boldsymbol{\gamma}$ as a function of $\mathbf{x}$ and $1/\alpha_s$ based on (28), and then estimate $\mathbf{x}$ based on (27) by plugging in the estimate of $\boldsymbol{\gamma}$. From (28), the LS estimate of $\boldsymbol{\gamma}$ is given by

$$\hat{\boldsymbol{\gamma}} = (\mathbf{F}^T\mathbf{F})^{-1}\left(\frac{1}{\alpha_s}cT_I(\mathbf{q} - \mathbf{u})\right.$$
$$\left. + \mathbf{F}_3^T(\mathbf{d} + (d_M + \Delta)\mathbf{1}_M - \mathbf{d}_a)\right). \quad (29)$$

Plugging (29) into (27), and rearranging the terms, we achieve

$$\mathbf{K}_1(\mathbf{d} + (d_M + \Delta)\mathbf{1}_M - \mathbf{d}_a)$$
$$= \frac{1}{\alpha_s}cT_I\mathbf{F}_3(\mathbf{F}^T\mathbf{F})^{-1}(\mathbf{q} - \mathbf{u}) \quad (30)$$

where $\mathbf{K}_1 = \mathbf{I}_M - \mathbf{F}_3(\mathbf{F}^T\mathbf{F})^{-1}\mathbf{F}_3^T$, which is full rank, and whose inverse is explored in Appendix A. Premultiplying both sides of (30) with $\mathbf{K}_1^{-1}$, we arrive at

$$\mathbf{d} + (d_M + \Delta)\mathbf{1}_M - \mathbf{d}_a = \frac{1}{\alpha_s}\mathbf{h} \quad (31)$$

where $\mathbf{h} = cT_I\mathbf{K}_1^{-1}\mathbf{F}_3(\mathbf{F}^T\mathbf{F})^{-1}(\mathbf{q} - \mathbf{u})$. We remark that at this point an MLE can be derived to jointly estimate $\mathbf{x}$, Δ and $1/\alpha_s$ based on (31) via exhaustive search. It needs at least four anchors to locate a target node on a plane in this case. However, it has a high computational complexity. Thus, we continue to investigate low-complexity closed-form solutions. Applying $\mathbf{P}$ to get rid of $(d_M + \Delta)\mathbf{1}_M$, recalling that $\mathbf{P}\mathbf{d} = \mathbf{d} - \bar{d}\mathbf{1}_M$, and moving $\mathbf{d}$ to one side and the other terms to the other side, we obtain

$$\mathbf{d} = \frac{1}{\alpha_s}\mathbf{P}\mathbf{h} + \bar{d}\mathbf{1}_M + \mathbf{P}\mathbf{d}_a. \quad (32)$$

Executing element-wise multiplication and rearranging the equation, we obtain the linear equation

$$\boldsymbol{\phi} = \mathbf{H}\mathbf{s}, \tag{33}$$

where

$$\boldsymbol{\phi} = \boldsymbol{\psi}_a - (\mathbf{P}\mathbf{d}_a) \odot (\mathbf{P}\mathbf{d}_a),$$
$$\mathbf{s} = [\mathbf{x}^T, \bar{d}, 1/\alpha_s, \bar{d}^2 - \|\mathbf{x}\|^2, 1/\alpha_s^2, 2\bar{d}/\alpha_s]^T$$

and

$$\mathbf{H} = [2\mathbf{X}_a^T, 2\mathbf{P}\mathbf{d}_a, 2(\mathbf{P}\mathbf{h}) \odot (\mathbf{P}\mathbf{d}_a), \mathbf{1}_M, (\mathbf{P}\mathbf{h}) \odot (\mathbf{P}\mathbf{h}), \mathbf{P}\mathbf{h}].$$

However, as investigated in Appendix B, $\mathbf{H}$ is always rank-deficient in the noiseless case or with sufficiently small noise. Hence, it is impossible to have a unique estimate of $\mathbf{s}$ based on (33). We can also interpret this problem from another point of view. Our method is equivalent to first jointly estimating $\boldsymbol{\gamma}$, $\mathbf{d}$, $1/\alpha_s$, and $d_M + \Delta$ (in total $2M + 2$ parameters) based on (25)–(27), then plugging the estimate of $\boldsymbol{\gamma}$ into (27), linearizing the equations w.r.t. $\mathbf{x}$, and finally estimating $\mathbf{x}$. But (25) and (26) are linearly dependent in the noiseless case or with sufficiently small noise, and there are only $2M$ independent equations in (25)–(27). Therefore, we cannot estimate $\boldsymbol{\gamma}$ without ambiguities, and that is why (33) does not have a unique solution.

However, let us take some practical issues into account to solve this problem. The clock skew of the ith anchor relative to the absolute time is $\alpha_i - 1$, which is in the order of several tens of ppm (10^{-6}). The typical range of $\alpha_i - 1$ is from 2 ppm to 80 ppm according to the standard, which means that α_i is in the range of 0.99992 to 1.00008, and also α_s is in the same range. Thus, we can make a first-order Taylor expansion of $1/\alpha_s^2$ as a function of $1/\alpha_s$ around 1 by ignoring the higher order terms as $1/\alpha_s^2 \approx 2/\alpha_s - 1$. We can plug it into (33), rearrange the terms, and then obtain an equation w.r.t. $\mathbf{x}$, $\bar{d}$, $\bar{d}/\alpha_s$, $1/\alpha_s$ and $\bar{d}^2 - \|\mathbf{x}\|^2$ (in total $l + 4$ unknowns). However, if we make further use of the prior knowledge that α_s is very close to 1, we can obtain an equation with even fewer unknowns, leading to a better estimation performance. Thus, we can further assume that $\bar{d}/\alpha_s \approx \bar{d}$, and plug this together with $1/\alpha_s^2 \approx 2/\alpha_s - 1$ into (33), which leads to

$$\boldsymbol{\phi}_d = \mathbf{H}_d \mathbf{s}_d \tag{34}$$

where $\boldsymbol{\phi}_d = \boldsymbol{\phi} + (\mathbf{P}\mathbf{h}) \odot (\mathbf{P}\mathbf{h})$, $\mathbf{s}_d = [\mathbf{x}^T, \bar{d}, 1/\alpha_s, \bar{d}^2 - \|\mathbf{x}\|^2]^T$ and $\mathbf{H}_d = [2\mathbf{X}_a^T, 2\mathbf{P}(\mathbf{d}_a + \mathbf{h}), 2\mathbf{P}\mathbf{h} \odot (\mathbf{P}\mathbf{d}_a + \mathbf{P}\mathbf{h}), \mathbf{1}_M]$. Note that there are only $l + 3$ unknowns in (34). The LS estimate of $\mathbf{s}_d$ is then given by

$$\hat{\mathbf{s}}_d = (\mathbf{H}_d^T \mathbf{H}_d)^{-1} \mathbf{H}_d^T \boldsymbol{\phi}. \tag{35}$$

Note that the rank of $\mathbf{H}_d$ should be $l + 3$ in order to estimate all the parameters, which indicates $M - 1 \geq l + 3$. It needs at least six anchors to estimate all the parameters in a plane.

Now that we can simplify the problem by considering practical issues, let us revisit the data model (32). Since α_s is very close to 1, we may assume $\frac{1}{\alpha_s}\mathbf{P}\mathbf{h} \approx \mathbf{P}\mathbf{h}$ by ignoring the effect of $1/\alpha_s$, which means we treat α_s as 1, although it may not

be exactly equal to 1. Note that this approximation can be improved by first applying conventional synchronization methods to the target node. We can then rewrite (32) as

$$\mathbf{d} \approx \mathbf{P}\mathbf{h} + \bar{d}\mathbf{1}_M + \mathbf{P}\mathbf{d}_a. \tag{36}$$

Sequentially, after element-wise multiplication and moving terms, we arrive at

$$\boldsymbol{\phi}_a = \mathbf{H}_a \mathbf{s}_a \tag{37}$$

where $\boldsymbol{\phi}_a = \boldsymbol{\psi}_a - (\mathbf{P}(\mathbf{d}_a + \mathbf{h})) \odot (\mathbf{P}(\mathbf{d}_a + \mathbf{h}))$, $\mathbf{s}_a = [\mathbf{x}^T, \bar{d}, \bar{d}^2 - \|\mathbf{x}\|^2]^T$, and $\mathbf{H}_a = [2\mathbf{X}_a^T, 2\mathbf{P}(\mathbf{d}_a + \mathbf{h}), \mathbf{1}_M]$. The LS estimate of $\mathbf{s}_a$ is then given by

$$\hat{\mathbf{s}}_a = (\mathbf{H}_a^T \mathbf{H}_a)^{-1} \mathbf{H}_a^T \boldsymbol{\phi}_a. \tag{38}$$

The rank of $\mathbf{H}_a$ should be $l + 2$ in order to estimate all the parameters, which indicates $M - 1 \geq l + 2$. It needs at least five anchors to estimate all the parameters in a plane. As a result, taking such practical issues into account can dramatically simplify the problem. Moreover, we remark that the data model (36) is similar to the data model (7) in Section III-B. Thus, the localization algorithms in Section III-B for quasi-synchronous networks can also be applied here to estimate $\mathbf{x}$.

Since it is always complicated to estimate $\boldsymbol{\gamma}$ and $\mathbf{x}$ jointly, we can also resort to simple solutions to decouple the synchronization and the localization. Defining $\boldsymbol{\beta} = \alpha_M[1/\alpha_1, 1/\alpha_2, \ldots, 1/\alpha_{M-1}]^T$ of length $M - 1$, and $\tilde{\boldsymbol{\beta}} = [\boldsymbol{\beta}^T, \alpha_M/\alpha_s]^T$ of length M, we can first estimate $\tilde{\boldsymbol{\beta}}$ based on (25) and (26), which means that we first make use of T_I between the two RMARKERs to Calibrate the Clock Skews, and then Estimate the Node Position (CCS-ENP). As α_M is tightly coupled with the other clock skews, we can only estimate their ratios. We combine (25) and (26) ignoring the noise terms as

$$\mathbf{F}_\beta \tilde{\boldsymbol{\beta}} = \mathbf{b}_\beta \tag{39}$$

where $\mathbf{b}_\beta = [cT_I \mathbf{1}_{M-1}^T, \mathbf{0}_{M-1}^T, q_M - u_M]^T$, and

$$\mathbf{F}_\beta = \begin{bmatrix} \mathbf{Z}\mathbf{F}_1\mathbf{Z}^T & \mathbf{0}_{M-1} \\ \mathbf{Z}\mathbf{F}_2\mathbf{Z}^T & -cT_I\mathbf{1}_{M-1} \\ \mathbf{0}_{M-1}^T & -cT_I \end{bmatrix}. \tag{40}$$

Consequently, the LS estimates of $\tilde{\boldsymbol{\beta}}$ and $\boldsymbol{\beta}$ are given by

$$\hat{\tilde{\boldsymbol{\beta}}} = (\mathbf{F}_\beta^T \mathbf{F}_\beta)^{-1} \mathbf{F}_\beta^T \mathbf{b}_\beta, \tag{41}$$
$$\hat{\boldsymbol{\beta}} = \mathbf{Z}\hat{\tilde{\boldsymbol{\beta}}}, \tag{42}$$

respectively. Since only (27) is related to $\mathbf{x}$, we rewrite it as an equation in $\boldsymbol{\beta}$ and $\mathbf{x}$ without noise terms

$$\mathbf{F}_3\boldsymbol{\beta}_1 = \alpha_M(\mathbf{d} - \mathbf{d}_a + (d_M + \Delta)\mathbf{1}_M) \tag{43}$$

where $\boldsymbol{\beta}_1 = [\boldsymbol{\beta}^T, 1]^T$. Due to the fact that $\alpha_M \approx 1$, we can write $\alpha_M\mathbf{d} \approx \mathbf{d}$ and $\alpha_M\mathbf{d}_a \approx \mathbf{d}_a$. Thus, we can rewrite (43) as

$$\mathbf{F}_3\boldsymbol{\beta}_1 \approx \mathbf{d} + (d_M + \alpha_M\Delta)\mathbf{1}_M - \mathbf{d}_a \tag{44}$$

where α_M is tightly coupled with Δ. Again, we can improve this approximation by first synchronizing the Mth anchor in order to improve the localization performance. Plugging $\hat{\boldsymbol{\beta}}$ into (44), we observe that it is equivalent to the position estimation

based on (5). Therefore, the time-based localization algorithms in Section III.B for quasi-synchronous networks can again be applied here to estimate **x**. For brevity, we do not repeat the algorithms here. We remark that employing this separate method, we also need five anchors to calibrate the clock skews and estimate the target position in a plane. As an extension, even if some of the anchors are manipulated by attackers to report misinformation, we could still combine our approach with the methods in [39] or [40] to mitigate the influence of outliers. This is left for future work.

V. PERFORMANCE BOUNDS AND NUMERICAL RESULTS

As a well-adopted lower bound, the Cramèr-Rao bound (CRB) is derived for quasi-synchronous and fully asynchronous networks, respectively. Here, we exemplify the CRBs for location estimation on a plane, e.g., we take $l = 2$. The Fisher information matrix (FIM) $\mathbf{I}_1(\boldsymbol{\theta}_1)$ based on the model (5) in Section III-A for quasi-synchronous networks is derived in Appendix C, where $\boldsymbol{\theta}_1 = [\Delta, \mathbf{x}^T]^T$, and $\mathbf{x} = [x_1, x_2]^T$. Consequently, we obtain $\text{CRB}(x_1) = [\mathbf{I}_1^{-1}(\boldsymbol{\theta}_1)]_{2,2}$ and $\text{CRB}(x_2) = [\mathbf{I}_1^{-1}(\boldsymbol{\theta}_1)]_{3,3}$. We observe that Δ is not part of $\mathbf{I}_1^{-1}(\boldsymbol{\theta}_1)$. Therefore, no matter how large Δ is, it has the same influence on the CRB for quasi-synchronous networks. On the other hand, the FIM $\mathbf{I}_2(\boldsymbol{\theta}_2)$ based on the model (25)–(27) in Section IV-A for fully asynchronous networks is derived in Appendix D, where $\boldsymbol{\theta}_2 = [\mathbf{x}^T, \Delta, \boldsymbol{\alpha}^T, 1/\alpha_s]^T$, and $\boldsymbol{\alpha} = [\alpha_1, \alpha_2, \ldots, \alpha_M]^T$. As a result, we achieve $\text{CRB}(x_1) = [\mathbf{I}_2^{-1}(\boldsymbol{\theta}_2)]_{1,1}$ and $\text{CRB}(x_2) = [\mathbf{I}_2^{-1}(\boldsymbol{\theta}_2)]_{2,2}$. All the parameters of $\boldsymbol{\theta}_2$ appear in $\mathbf{I}_2(\boldsymbol{\theta}_2)$, and thus they all influence the CRB for fully asynchronous networks.

Let us now evaluate the performance of the proposed robust localization algorithms by Monte Carlo simulations, and compare it with the CRB. We consider two simulation setups: Setup 1 and Setup 2. In Setup 1, the anchors are evenly located on the edges of a 40 m × 40 m rectangular to mimic an indoor geometry scale. Meanwhile the target node is randomly located on a grid with cells of size 1 m × 1 m inside the rectangular. In Setup 2, all anchors and the target node are randomly distributed on the grid inside the rectangular. Furthermore, n_{iR} and m_{iR} have the same variance σ_{iR}^2, while n_{iS} and m_{iS} have the same variance σ_{iS}^2. Due to the broadcast property of the ranging protocol, we assume that σ_{iS}^2 and σ_{iR}^2 are related to the distances according to the path loss law. Thus we define the average noise power as $\bar{\sigma}^2 = 1/M \sum_{i=1}^{M} \sigma_{iS}^2$, where σ_{iR}^2 and σ_{iS}^2 are chosen to fulfill the condition that all σ_{iR}^2/d_{iM}^2 and σ_{iS}^2/d_i^2 are equal as in [9]. Note that since $d_{MM} = 0$, we simply assume $\sigma_{MR}^2 = 0$ and $n_{MR} = 0$. The processing time of the target node is 5 ms, and as a result the corresponding distance Δ is $3 \times 10^8 \times 5 \times 10^{-3} = 1.5 \times 10^6$ m. The time interval T_I between RMARKER1 and RMARKER2 is 1 ms. The clock skews of the anchors and the target are randomly generated in the range of $[1-100\,\text{ppm}, 1+100\,\text{ppm}]$. The performance criterion is the root mean square error (RMSE) of $\hat{\mathbf{x}}$ versus SNR, which can be expressed as $\sqrt{1/N_{\text{exp}} \sum_{j=1}^{N_{\text{exp}}} \|\hat{\mathbf{x}}^{(j)} - \mathbf{x}\|^2}$, where $\hat{\mathbf{x}}^{(j)}$ is the estimate obtained in the jth trial. Each simulation result is averaged over $N_{\text{exp}} = 1000$ Monte Carlo trials. We would like to
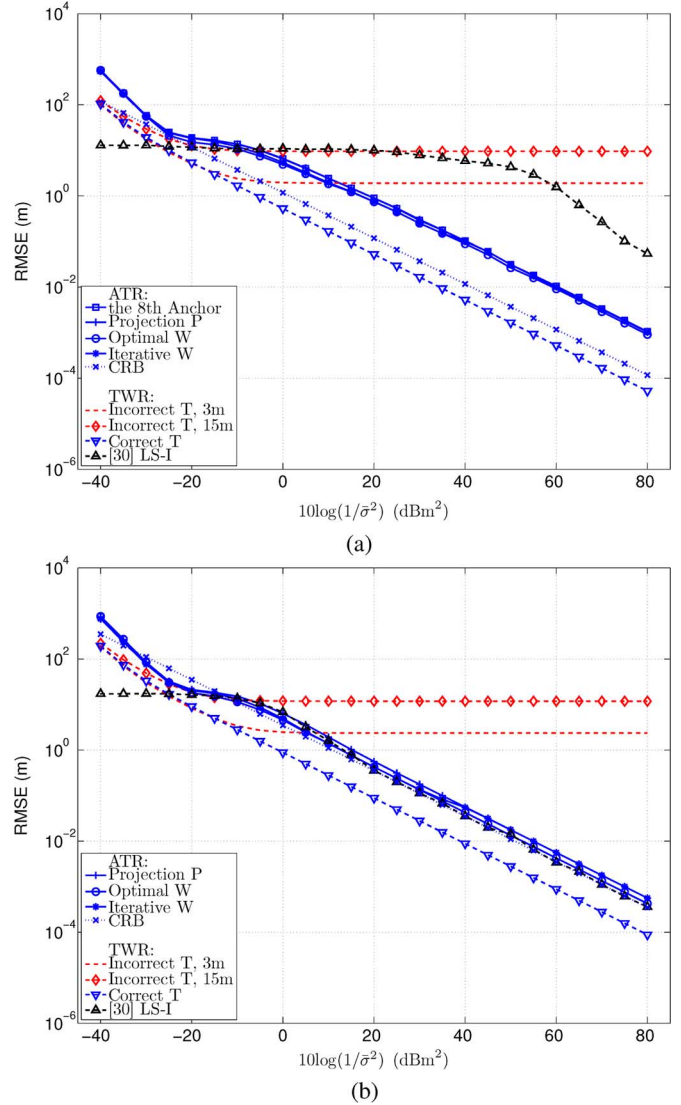

Fig. 4. RMSE of target node position **x** for quasi-synchronous networks. (a) Setup 1, $M = 8$. (b) Setup 2, $M = 8$.

compare our localization algorithms with the conventional localization algorithm using the TWR protocol, which is clarified in Appendix E, and the algorithm LS-I in [30]. We assume that the algorithm LS-I in [30] is employed with accurate knowledge of the anchor clock parameters and positions. The number of rounds of two-way message exchanges for LS-I in [30] is four, as with more than four rounds, the estimation performance improvement is only marginal [30]. The clock offsets are randomly generated in the range of [1 ns, 10 ns].

A. Localization for Quasi-Synchronous Networks

Fig. 4(a) and (b) shows the localization performance of respectively Setup 1 and Setup 2 with eight anchors that do not suffer from clock skews. In each Monte Carlo run, we generate a new geometry. In both figures, the dashed lines with no and "◇" markers represent the conventional localization algorithm using the fraudulent timestamp report from the target node with 3 m and 15 m errors, respectively. According to the figures,

they cannot estimate the target position correctly even with sufficiently small noise terms. A larger timestamp error introduces a higher error floor. The dashed line with "∇" markers illuminates the conventional localization algorithm using the correct timestamp report. It is slightly better than the CRB of our method for Setup 1 (the dotted line with "×" markers), but much better than the one for Setup 2. This is reasonable, since the conventional method estimates less parameters than the proposed method. The performance of the algorithm LS-I (the dashed line with "△" markers) in Setup 1 and Setup 2 is quite different. It is worse than our method (the solid lines with different markers) in Setup 1, whereas it is better than our method in Setup 2. As a result, the algorithm LS-I seems to be sensitive to the geometry, when the target node is inside the region restricted by the anchors. Moreover, $8M$ ranging packets are transmitted in the algorithm LS-I compared to only 2 ranging packets in our scheme, so our communication load is much smaller. Furthermore, the method in Section III-B is immune to a fraudulent timestamp report and robust to the randomness of the target node clock. Moreover, its localization performance is accurate with sufficiently small noise terms. The solid line with "□" markers shows the performance of the LS estimator using the eighth anchor as the reference node [44], whereas the solid line with "+" markers indicates the performance of our proposed LS estimator using the projection $\mathbf{P}$. Note that they almost overlap. The solid lines with "o" and "∗" markers denote the performance of our proposed WLS method with an optimal weighting and an iterative weighting matrix, respectively. The fact that they almost overlap indicates that if we use the LS estimate as an initial point, the iterative WLS can converge to the WLS with optimal weighting. The performance of the WLS with optimal weighting is slightly better than the LS and the iterative WLS estimators. Considering the computational complexity and the performance, the LS estimator would be the best option.

B. Localization for Fully Asynchronous Networks

Fig. 5(a) and (b) illustrates the localization performance of respectively Setup 1 and Setup 2 with eight anchors in fully asynchronous networks. The dotted lines with "◇" markers depict the performance of the conventional TWR algorithm without clock skew calibration. The high error floors indicate that it cannot estimate the correct position of the target even with sufficiently small noise. The dotted line with "∇" markers indicates the performance of the conventional TWR algorithm using a correct timestamp report and with clock skew calibration. It is lower than the dotted line with "×" markers, which represents the CRB and serves as a benchmark for fully asynchronous networks. There are performance gaps between the CRB and the proposed methods in both figures. However, the gap is smaller in Setup 2. The proposed methods make a tradeoff between performance and complexity. The performance of the algorithm LS-I (the dashed line with "△" markers) in Setup 1 and Setup 2 is again quite different. It is slightly worse than our method (the solid lines with different markers) in Setup 1, whereas it is better than the CRB in Setup 2. Note that it estimates much fewer parameters than ours, since it assumes the exact knowledge of the
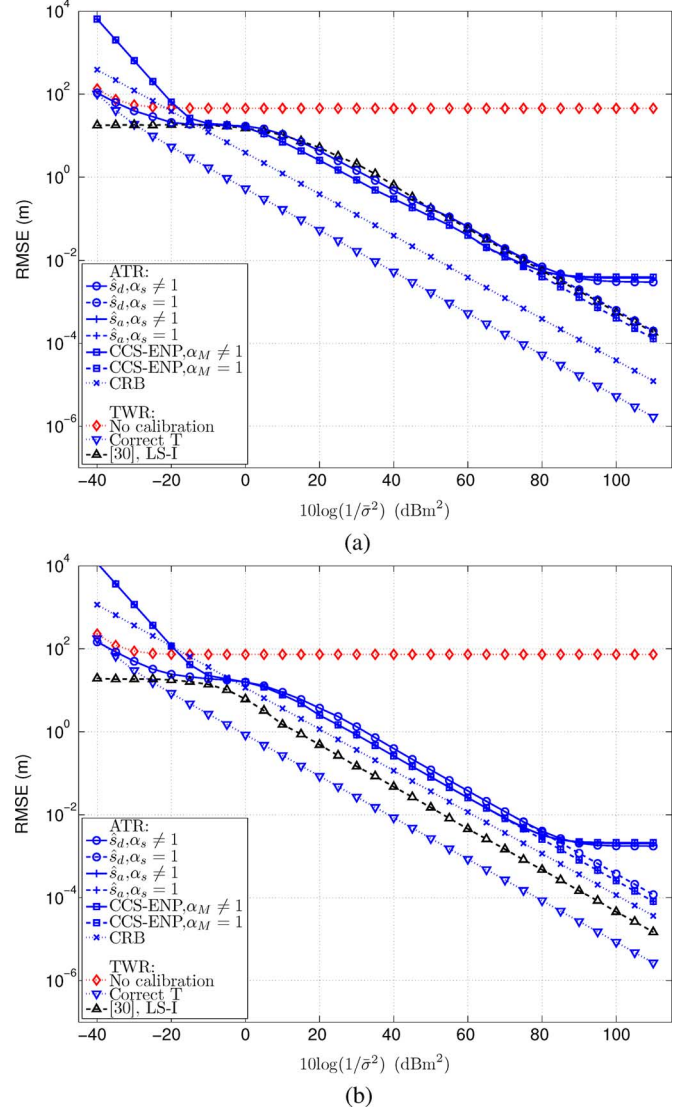

Fig. 5. RMSE of target node position $\mathbf{x}$ for fully asynchronous networks. (a) Setup 1, $M = 8$. (b) Setup 2, $M = 8$.

anchor clock parameters. On the other hand, we estimate the anchor clock skews and the target node position together. The algorithm LS-I still seems to be sensitive to the geometry, and has much more communication load than ours. The estimator $\hat{\mathbf{s}}_a$ (the lines with "+" markers) and the CCS-ENP method (the lines with "□" markers) achieve the same performance. The performance of the estimator $\hat{\mathbf{s}}_d$ (the lines with "o" markers) is worse than them in general, as it estimates more parameters. Note that $\hat{\mathbf{s}}_a$ treats α_s as 1, and $\hat{\mathbf{s}}_d$ treats $1/\alpha_s^2$ as $2/\alpha_s - 1$ and $\bar{d}/\alpha_s$ as $\bar{d}$. Therefore, there are error floors when $\alpha_s \neq 1$ (the solid lines with "+" and "o" markers), but these floors only appear at high SNR. The performance degradation at high SNR caused by the approximation error in $\hat{\mathbf{s}}_a$ is more important than the benefit of less unknowns. Thus, $\hat{\mathbf{s}}_a$ has a slightly higher error floor than $\hat{\mathbf{s}}_d$ when $\alpha_s \neq 1$ at high SNR. However, as long as the condition $\alpha_s = 1$ is fulfilled, both $\hat{\mathbf{s}}_a$ and $\hat{\mathbf{s}}_d$ (the dashed lines with "+" and "o" markers) can achieve accurate estimates, even for high SNR. The CCS-ENP method is developed by treating α_M as 1. Thus, it has a similar error floor at high SNR when $\alpha_M \neq 1$,

which is indicated by the solid line with "□" markers. Based on the above analysis, both the estimator $\hat{\mathbf{s}}_a$ and the CCS-ENP method are good choices considering the implementation cost and performance.

VI. CONCLUSION

In this paper, we have proposed robust localization strategies based on TOA measurements to localize a target node with the help of anchors for asynchronous networks. We have dealt with two kinds of asynchronous networks: one with only clock offsets referred to as quasi-synchronous networks, and the other not only with clock offsets but also clock skews referred to as fully asynchronous networks. Regardless of the reliability of the timestamps from the target node, we have proposed a novel ranging protocol, namely asymmetric trip ranging (ATR), which leads to localization methods that are naturally immune to internal attacks mounted by a compromised target node. LS and WLS estimators have been proposed to localize the target node for quasi-synchronous networks. For fully asynchronous networks, we have also developed closed-form LS estimators to jointly estimate the position and clock parameters taking practical issues into account. Furthermore, we have decoupled localization and synchronization, and proposed a simple yet efficient method, which is to first **C**alibrate the **C**lock **S**kews, and then **E**stimate the **N**ode **P**osition (CCS-ENP). Moreover, the CRBs for both quasi-synchronous and fully asynchronous networks have been derived, respectively. Simulation results have corroborated the efficiency of our localization methods. In future work, we can formulate a total least squares (TLS) estimator taking the inaccuracies of the anchor position and clock parameters into account, when we use located target nodes as new anchors to localize other target nodes in large WSNs.

APPENDIX A
COMPUTATION OF $\mathbf{K}^{-1}$

Since $\mathbf{K}_1 = \mathbf{I}_M - \mathbf{F}_3(\mathbf{F}^T\mathbf{F})^{-1}\mathbf{F}_3^T$, $\mathbf{K}_1^{-1}$ can be written as

$$
\begin{aligned}
\mathbf{K}_1^{-1} &= \left(\mathbf{I}_M - \mathbf{F}_3(\mathbf{F}^T\mathbf{F})^{-1}\mathbf{F}_3^T\right)^{-1} \\
&= \left(\mathbf{I}_M - \left(\left(\mathbf{F}_3^T\right)^{-1}(\mathbf{F}^T\mathbf{F})\mathbf{F}_3^{-1}\right)^{-1}\right)^{-1} \\
&= \left(\mathbf{F}_3^T\right)^{-1}(\mathbf{F}^T\mathbf{F})\mathbf{F}_3^{-1}\left(\left(\mathbf{F}_3^T\right)^{-1}(\mathbf{F}^T\mathbf{F})\mathbf{F}_3^{-1} - \mathbf{I}_M\right)^{-1} \\
&= \left(\mathbf{F}_3^T\right)^{-1}(\mathbf{F}^T\mathbf{F})\left((\mathbf{F}_3^T)^{-1}(\mathbf{F}^T\mathbf{F}) - \mathbf{F}_3\right)^{-1} \\
&= \left(\mathbf{F}_3^T\right)^{-1}(\mathbf{F}^T\mathbf{F})\left(\mathbf{F}^T\mathbf{F} - \mathbf{F}_3^T\mathbf{F}_3\right)^{-1}\mathbf{F}_3^T.
\end{aligned} \tag{45}
$$

Recalling that $\mathbf{F} = [\mathbf{F}_1^T\mathbf{Z}^T - \mathbf{E}_1^T, \mathbf{F}_2^T, \mathbf{F}_3^T]^T$, we arrive at

$$
\begin{aligned}
\mathbf{F}^T\mathbf{F} - \mathbf{F}_3^T\mathbf{F}_3 &= \mathbf{F}_1^T\mathbf{Z}^T\mathbf{Z}\mathbf{F}_1 + \mathbf{F}_2^T\mathbf{F}_2 + \mathbf{E}_1^T\mathbf{E}_1 \\
&\quad - \mathbf{F}_1^T\mathbf{Z}^T\mathbf{E}_1 - \mathbf{E}_1^T\mathbf{Z}\mathbf{F}_1 \\
&= \begin{bmatrix} \mathbf{\Lambda} & \boldsymbol{\rho} \\ \boldsymbol{\rho}^T & f \end{bmatrix}
\end{aligned} \tag{46}
$$

where $\boldsymbol{\rho} = cT_I\mathbf{Z}(\mathbf{p} - \mathbf{v})$, $f = (M-1)c^2T_I^2 + [\mathbf{g}_2]_M$, $\mathbf{\Lambda} = \mathbf{Z}(\text{diag}(\mathbf{g}_1 + \mathbf{g}_2))\mathbf{Z}^T$, which is a diagonal matrix of size $(3M-$

$1) \times (3M-1)$ with $\mathbf{g}_1 = (\mathbf{p} - \mathbf{v}) \odot (\mathbf{p} - \mathbf{v})$ and $\mathbf{g}_2 = (\mathbf{q} - \mathbf{u}) \odot (\mathbf{q} - \mathbf{u})$. The inverse of $\mathbf{F}^T\mathbf{F} - \mathbf{F}_3^T\mathbf{F}_3$ is given by

$$
(\mathbf{F}^T\mathbf{F} - \mathbf{F}_3^T\mathbf{F}_3)^{-1} = \begin{bmatrix} \mathbf{\Lambda}^{-1} + \frac{1}{w}\mathbf{\Lambda}^{-1}\boldsymbol{\rho}\boldsymbol{\rho}^T\mathbf{\Lambda}^{-1} & \frac{1}{w}\mathbf{\Lambda}^{-1}\boldsymbol{\rho} \\ \frac{1}{w}\boldsymbol{\rho}^T\mathbf{\Lambda}^{-1} & \frac{1}{w} \end{bmatrix} \tag{47}
$$

where $w = f - \boldsymbol{\rho}^T\mathbf{\Lambda}^{-1}\boldsymbol{\rho}$. We further have

$$
\begin{aligned}
\mathbf{\Lambda}^{-1} &= \mathbf{Z}(\text{diag}(\mathbf{g}_1 + \mathbf{g}_2))^{-1}\mathbf{Z}^T, \\
\mathbf{\Lambda}^{-1}\boldsymbol{\rho} &= cT_I\mathbf{Z}(\text{diag}(\mathbf{g}_1 + \mathbf{g}_2))^{-1}\mathbf{Z}^T\mathbf{Z}(\mathbf{p} - \mathbf{v}), \\
\mathbf{\Lambda}^{-1}\boldsymbol{\rho}\boldsymbol{\rho}^T\mathbf{\Lambda}^{-1} &= c^2T_I^2\mathbf{Z}(\text{diag}(\mathbf{g}_1 + \mathbf{g}_2))^{-1}\mathbf{Z}^T\mathbf{Z} \\
&\quad \times (\mathbf{p} - \mathbf{v})(\mathbf{p} - \mathbf{v})^T\mathbf{Z}^T\mathbf{Z}(\text{diag}(\mathbf{g}_1 + \mathbf{g}_2))^{-1}\mathbf{Z}^T, \\
\boldsymbol{\rho}^T\mathbf{\Lambda}^{-1}\boldsymbol{\rho} &= c^2T_I^2(\mathbf{p} - \mathbf{v})^T\mathbf{Z}^T\mathbf{Z} \\
&\quad \times (\text{diag}(\mathbf{g}_1 + \mathbf{g}_2))^{-1}\mathbf{Z}^T\mathbf{Z}(\mathbf{p} - \mathbf{v}).
\end{aligned}
$$

$\mathbf{K}_1^{-1}$ can be obtained by plugging the expression of $(\mathbf{F}^T\mathbf{F} - \mathbf{F}_3^T\mathbf{F}_3)^{-1}$ into (45).

APPENDIX B
COMPUTATION OF $\mathbf{H}$

In the noiseless case or with sufficiently small noise, $\mathbf{Ph} = \alpha_s(\mathbf{Pd} - \mathbf{Pd}_a)$. Recalling that $\mathbf{H} = [2\mathbf{X}_a^T, 2\mathbf{Pd}_a, 2(\mathbf{Ph}) \odot (\mathbf{Pd}_a), \mathbf{1}_M, (\mathbf{Ph}) \odot (\mathbf{Ph}), \mathbf{Ph}]$, we explore the properties of $\mathbf{H}$. With $\mathbf{Pd} = \mathbf{d} - \bar{d}\mathbf{1}_M$, $\mathbf{Pd}_a = \mathbf{d}_a - \bar{d}_a\mathbf{1}_M$ (where $\bar{d}_a = \frac{1}{M}\sum_{i=1}^M d_{iM}$), $\mathbf{d} \odot \mathbf{d} = \boldsymbol{\psi}_a - 2\mathbf{X}_a^T\mathbf{x} + \|\mathbf{x}\|^2\mathbf{1}_M$, and $\mathbf{d}_a \odot \mathbf{d}_a = \boldsymbol{\psi}_a - 2\mathbf{X}_a^T\mathbf{x}_M + \|\mathbf{x}_M\|^2\mathbf{1}_M$, we obtain

$$
\begin{aligned}
&\mathbf{Pd} \odot \mathbf{Pd}_a \\
&\quad = \mathbf{d}_a \odot \mathbf{d} - \bar{d}_a\mathbf{d} - \bar{d}\mathbf{d}_a + \bar{d}_a\bar{d}\mathbf{1}_M \tag{48} \\
&(\mathbf{Ph}) \odot (\mathbf{Pd}_a) \\
&\quad = \alpha_s(\mathbf{Pd} - \mathbf{Pd}_a) \odot (\mathbf{Pd}_a) \tag{49} \\
&\quad = \alpha_s(\mathbf{d}_a \odot \mathbf{d} - \mathbf{d}_a \odot \mathbf{d}_a - \bar{d}_a\mathbf{d} \\
&\qquad - (\bar{d} + 2\bar{d}_a)\mathbf{d}_a + (\bar{d}_a\bar{d} - \bar{d}_a^2)\mathbf{1}_M), \\
&\mathbf{Ph} \odot \mathbf{Ph} \\
&\quad = \alpha_s^2((\mathbf{Pd}) \odot (\mathbf{Pd}) - 2(\mathbf{Pd}) \odot (\mathbf{Pd}_a) \\
&\qquad + (\mathbf{Pd}_a) \odot (\mathbf{Pd}_a)) \\
&\quad = \alpha_s^2(\mathbf{d} \odot \mathbf{d} + \mathbf{d}_a \odot \mathbf{d}_a - 2\mathbf{d}_a \odot \mathbf{d} \\
&\qquad + (\bar{d}_a^2 + \bar{d}^2 - 2\bar{d}_a\bar{d})\mathbf{1}_M + 2(\bar{d} - \bar{d}_a)\mathbf{d}_a \\
&\qquad + 2(\bar{d}_a - \bar{d})\mathbf{d}). \tag{50}
\end{aligned}
$$

Based on (49) and (50), we have

$$
\begin{aligned}
&\mathbf{Ph} \odot \mathbf{Ph} + 2\alpha_s(\mathbf{Ph}) \odot (\mathbf{Pd}_a) \\
&\quad = \alpha_s^2\left(2\mathbf{X}_a^T(\mathbf{x}_M - \mathbf{x}) + \left(\|\mathbf{x}\|^2 - \|\mathbf{x}_M\|^2 + \bar{d}^2 - \bar{d}_a^2\right)\mathbf{1}_M \right. \\
&\qquad \left. - 6\bar{d}_a\mathbf{d}_a - 2\bar{d}\mathbf{d}\right). \tag{51}
\end{aligned}
$$

Consequently, the independent columns of $\mathbf{H}$ are $\mathbf{X}_a^T, \mathbf{1}_M, \mathbf{d}, \mathbf{d}_a, \mathbf{Ph} \odot \mathbf{Pd}_a$. The rank of $\mathbf{H}$ is $l + 4$, but its size is $M \times (l + 5)$. Thus, $\mathbf{H}$ is rank-deficient.

APPENDIX C
CRB DERIVATION FOR QUASI-SYNCHRONOUS NETWORKS

We analyze the CRB for jointly estimating Δ and $\mathbf{x}$ based on (5). The FIM $\mathbf{I}_1(\boldsymbol{\theta}_1)$ is employed, with entries defined as

$$[\mathbf{I}_1(\boldsymbol{\theta}_1)]_{ij} = -E\left[\frac{\partial^2}{\partial[\boldsymbol{\theta}_1]_i\partial[\boldsymbol{\theta}_1]_j}\ln p(\mathbf{u},\mathbf{v};\boldsymbol{\theta}_1)\right] \quad (52)$$

where $p(\mathbf{u},\mathbf{v};\boldsymbol{\theta}_1)$ is shown in (54). In the case of localization on a plane ($l = 2$), $\mathbf{I}_1(\boldsymbol{\theta}_1)$ can be specified as

$$\mathbf{I}_1(\boldsymbol{\theta}_1) = \begin{bmatrix} \mathbf{G} & \mathbf{r} \\ \mathbf{r}^T & k \end{bmatrix} \quad (53)$$

where $k = \sum_{i=1}^{M} 1/(\sigma_{iS}^2 + \sigma_{iR}^2)$, and $\mathbf{G}$ and $\mathbf{r}$ are defined in (55) and (56) at the bottom of the page, respectively.

$$p(\mathbf{u},\mathbf{v};\boldsymbol{\theta}_1) = \frac{1}{\sqrt{(2\pi)^M \prod_{i=1}^{M}(\sigma_{iS}^2 + \sigma_{iR}^2)}}$$
$$\times \exp\left(-\sum_{i=1}^{M}\frac{(u_i - v_i - d_i - d_M + d_{iM} - \Delta)^2}{2(\sigma_{iS}^2 + \sigma_{iR}^2)}\right). \quad (54)$$

APPENDIX D
CRB DERIVATION FOR FULLY ASYNCHRONOUS NETWORKS

We rewrite (25)–(27) as

$$\mathbf{Z}(\mathbf{p} - \mathbf{v}) = \frac{cT_I}{\alpha_M}\mathbf{Z}\boldsymbol{\alpha} + \mathbf{Z}(\mathbf{m}_r - \mathbf{n}_r), \quad (57)$$

$$\mathbf{q} - \mathbf{u} = \frac{cT_I}{\alpha_s}\boldsymbol{\alpha} + \mathbf{m}_s - \mathbf{n}_s, \quad (58)$$

$$\mathbf{u} - \mathbf{v} = \boldsymbol{\alpha} \odot (\mathbf{d} + (d_M + \Delta)\mathbf{1}_M - \mathbf{d}_a) + \mathbf{n}_s - \mathbf{n}_r. \quad (59)$$

We analyze the CRB for jointly estimating $\mathbf{x}$, Δ, $\boldsymbol{\alpha}$ and $1/\alpha_s$ based on (57)–(59). The FIM $\mathbf{I}_2(\boldsymbol{\theta}_2)$ is employed, with entries defined as

$$\mathbf{I}_2(\boldsymbol{\theta}_2) = -E\left[\frac{\partial^2 \ln p(\mathbf{u},\mathbf{v},\mathbf{p},\mathbf{q};\boldsymbol{\theta}_2)}{\partial\boldsymbol{\theta}_2\partial\boldsymbol{\theta}_2^T}\right]$$
$$= \left[\frac{\partial\boldsymbol{\mu}(\boldsymbol{\theta}_2)}{\partial\boldsymbol{\theta}_2}\right]^T \mathbf{C}^{-1}\left[\frac{\partial\boldsymbol{\mu}(\boldsymbol{\theta}_2)}{\partial\boldsymbol{\theta}_2}\right] \quad (60)$$

where

$$\boldsymbol{\mu}(\boldsymbol{\theta}_2) = \begin{bmatrix} (cT_I/\alpha_M)\mathbf{Z}\boldsymbol{\alpha} \\ (cT_I/\alpha_s)\boldsymbol{\alpha} \\ \boldsymbol{\alpha} \odot (\mathbf{d} + (d_M + \Delta)\mathbf{1}_M - \mathbf{d}_a) \end{bmatrix}, \quad (61)$$

$$\mathbf{C} = \begin{bmatrix} 2\mathrm{diag}(\mathbf{Z}\boldsymbol{\sigma}_r) & \mathbf{0}_{(M-1)\times M} & \mathbf{Z}\mathrm{diag}(\boldsymbol{\sigma}_r) \\ \mathbf{0}_{M\times(M-1)} & 2\mathrm{diag}(\boldsymbol{\sigma}_s) & \mathrm{diag}(\boldsymbol{\sigma}_s) \\ \mathrm{diag}(\boldsymbol{\sigma}_r)\mathbf{Z}^T & \mathrm{diag}(\boldsymbol{\sigma}_s) & \mathrm{diag}(\boldsymbol{\sigma}_r + \boldsymbol{\sigma}_s) \end{bmatrix} \quad (62)$$

where $\boldsymbol{\sigma}_r = [\sigma_{1R}^2, \sigma_{2R}^2, \ldots, \sigma_{(M-1)R}^2, 0]^T$ and $\boldsymbol{\sigma}_s = [\sigma_{1S}^2, \sigma_{2S}^2, \ldots, \sigma_{MS}^2]^T$. Furthermore, we achieve

$$\partial\boldsymbol{\mu}(\boldsymbol{\theta}_2)/\partial\Delta = [\mathbf{0}_{M-1}^T, \mathbf{0}_M^T, \boldsymbol{\alpha}^T]^T \quad (63)$$

$$\partial\boldsymbol{\mu}(\boldsymbol{\theta}_2)/\partial\frac{1}{\alpha_s} = [\mathbf{0}_{M-1}^T, -cT_I\boldsymbol{\alpha}^T, \mathbf{0}_M^T]^T \quad (64)$$

[see (65)–(66) at the bottom of the page]. We obtain $\partial\boldsymbol{\mu}(\boldsymbol{\theta}_2)/\partial\boldsymbol{\theta}_2$ by plugging in the above results. Then we can derive $\mathbf{I}_2(\boldsymbol{\theta}_2)$ based on (60).

$$\mathbf{G} =$$
$$\begin{bmatrix} \sum_{i=1}^{M}\frac{1}{\sigma_{iS}^2+\sigma_{iR}^2}\left(\frac{x_1-x_{1,i}}{\|\mathbf{x}-\mathbf{x}_i\|}+\frac{x_1-x_{1,M}}{\|\mathbf{x}-\mathbf{x}_M\|}\right)^2 & \sum_{i=1}^{M}\frac{1}{\sigma_{iS}^2+\sigma_{iR}^2}\left(\frac{x_1-x_{1,i}}{\|\mathbf{x}-\mathbf{x}_i\|}+\frac{x_1-x_{1,M}}{\|\mathbf{x}-\mathbf{x}_M\|}\right)\left(\frac{x_2-x_{2,i}}{\|\mathbf{x}-\mathbf{x}_i\|}+\frac{x_2-x_{2,M}}{\|\mathbf{x}-\mathbf{x}_M\|}\right) \\ \sum_{i=1}^{M}\frac{1}{\sigma_{iS}^2+\sigma_{iR}^2}\left(\frac{x_2-x_{2,i}}{\|\mathbf{x}-\mathbf{x}_i\|}+\frac{x_2-x_{2,M}}{\|\mathbf{x}-\mathbf{x}_M\|}\right)\left(\frac{x_1-x_{1,i}}{\|\mathbf{x}-\mathbf{x}_i\|}+\frac{x_1-x_{1,M}}{\|\mathbf{x}-\mathbf{x}_M\|}\right) & \sum_{i=1}^{M}\frac{1}{\sigma_{iS}^2+\sigma_{iR}^2}\left(\frac{x_2-x_{2,i}}{\|\mathbf{x}-\mathbf{x}_i\|}+\frac{x_2-x_{2,M}}{\|\mathbf{x}-\mathbf{x}_M\|}\right)^2 \end{bmatrix} \quad (55)$$

$$\mathbf{r} =$$
$$\left[\sum_{i=1}^{M}\frac{1}{\sigma_{iS}^2+\sigma_{iR}^2}\left(\frac{x_1-x_{1,i}}{\|\mathbf{x}-\mathbf{x}_i\|}+\frac{x_1-x_{1,M}}{\|\mathbf{x}-\mathbf{x}_M\|}\right) \quad \sum_{i=1}^{M}\frac{1}{\sigma_{iS}^2+\sigma_{iR}^2}\left(\frac{x_2-x_{2,i}}{\|\mathbf{x}-\mathbf{x}_i\|}+\frac{x_2-x_{2,M}}{\|\mathbf{x}-\mathbf{x}_M\|}\right)\right]^T. \quad (56)$$

$$[\partial\boldsymbol{\mu}(\boldsymbol{\theta}_2)/\partial\alpha_i]_j = \begin{cases} cT_I/\alpha_M, & j = i \text{ and } i \neq M \\ cT_I/\alpha_s, & j = i + M - 1 \\ d_i + d_M + \Delta - d_{iM}, & j = i + 2M - 1 \\ 0 & \text{else} \end{cases}$$
$$\text{for } i = 1, \ldots, M, \quad j = 1, \ldots, 3M - 1 \quad (65)$$

$$[\partial\boldsymbol{\mu}(\boldsymbol{\theta}_2)/\partial x_i]_j = \begin{cases} \alpha_{j+1-2M}\left(\frac{x_i-x_{i,j+1-2M}}{\|\mathbf{x}-\mathbf{x}_{j+1-2M}\|}+\frac{x_i-x_{i,M}}{\|\mathbf{x}-\mathbf{x}_M\|}\right), & 2M \leq j \leq 3M - 1 \\ 0, & \text{else} \end{cases}$$
$$\text{for } i = 1, \ldots, l, \quad j = 1, \ldots, 3M - 1. \quad (66)$$

APPENDIX E
CONVENTIONAL LOCALIZATION BY THE TWR PROTOCOL

Assume the distances between the target and the anchor nodes are measured by executing the TWR protocol. For each execution, we obtain four timestamps, namely T_{iS} and T_{iT} (the time when the RMARKER leaves the ith anchor), and $T_{ST}^{(i)}$ and $T_{SR}^{(i)}$ at the target. Recalling the parameters defined in the previous sections, the relations between the timestamps can be described as follows:

$$c(T_{iS} - T_{iT}) = 2d_i + \Delta + n_{iS} - n_{iT} \tag{67}$$

$$c(T_{ST}^{(i)} - T_{SR}^{(i)}) = \Delta + n_{ST}^{(i)} - n_{SR}^{(i)} \tag{68}$$

where we assume that exact knowledge of the time when the RMARKER leaves, thus $n_{iT} = n_{ST}^{(i)} = 0$, and $n_{SR}^{(i)}$ is a zero-mean random variable with the same variance σ_{iS}^2 as n_{iS}. We first obtain an estimate of Δ based on (68)

$$\hat{\Delta} = \frac{1}{M} \sum_{i=1}^{M} c(T_{ST}^{(i)} - T_{SR}^{(i)}). \tag{69}$$

Plugging (69) into (67), we can write (67) in vector form without noise terms as

$$\mathbf{u} - \mathbf{w} = 2\mathbf{d} + \hat{\Delta}\mathbf{1}_M \tag{70}$$

where $\mathbf{w} = [T_{1T}, T_{2T}, \dots, T_{MT}]^T$. The target position can then be estimated based on (70) using the same LS estimator as in Section III.

REFERENCES

[1] I. Akyildiz, W. Su, Y. Sankarasubramaniam, and E. Cayirci, "A survey on sensor networks," *IEEE Commun. Mag.*, vol. 40, no. 8, pp. 102–114, Aug. 2002.

[2] K. Langendoen and N. Reijers, "Distributed localization in wireless sensor networks: A quantitative comparison," *Comput. Netw.*, vol. 43, no. 4, pp. 499–518, Nov. 2003.

[3] N. Patwari, J. Ash, S. Kyperountas, I. Hero, A. O. , R. Moses, and N. Correal, "Locating the nodes: Cooperative localization in wireless sensor networks," *IEEE Signal Process. Mag.*, vol. 22, no. 4, pp. 54–69, Jul. 2005.

[4] S. Gezici, Z. Tian, G. Giannakis, H. Kobayashi, A. Molisch, H. Poor, and Z. Sahinoglu, "Localization via ultra-wideband radios: A look at positioning aspects for future sensor networks," *IEEE Signal Process. Mag.*, vol. 22, pp. 70–84, Jul. 2005.

[5] A. Sayed, A. Tarighat, and N. Khajehnouri, "Network-based wireless location: Challenges faced in developing techniques for accurate wireless location information," *IEEE Signal Process. Mag.*, vol. 22, no. 4, pp. 24–40, Jul. 2005.

[6] N. Niculescu and B. Nath, "Ad hoc positioning system (APS)," in *Proc. IEEE GlobeCom*, San Antonio, TX, Nov. 2001, pp. 2926–2931.

[7] Y. Shang, W. Ruml, Y. Zhang, and M. Fromherz, "Localization from mere connectivity," in *Proc. ACM MobiHoc*, Annapolis, MD, Jun. 2003, pp. 201–212.

[8] T. He, C. Huang, B. M. Blum, J. A. Stankovic, and T. Adbdelzaher, "Range-free localization schemes for large scale sensor networks," in *Proc. ACM MobiCom*, San Diego, CA, Sept. 2003, pp. 81–95.

[9] K. Cheung, H. So, W.-K. Ma, and Y. Chan, "Least squares algorithms for time-of-arrival-based mobile location," *IEEE Trans. Signal Process.*, vol. 52, no. 4, pp. 1121–1130, Apr. 2004.

[10] Y. Huang, J. Benesty, G. Elko, and R. Mersereati, "Real-time passive source localization: A practical linear-correction least-squares approach," *IEEE Trans. Acoust., Speech, Signal Process.*, vol. 9, no. 8, pp. 943–956, Nov. 2001.

[11] A. Savvides, C.-C. Han, and M. B. Strivastava, "Dynamic fine-grained localization in ad-hoc networks of sensors," in *Proc. ACM MobiCom*, Rome, Italy, Jul. 2001, pp. 166–179.

[12] D. Niculescu and B. Nath, "Ad hoc positioning system (APS) using AOA," in *Proc. IEEE INFOCOM*, San Francisco, CA, Apr. 2003, vol. 3, pp. 1734–1743.

[13] P. Bahl and V. Padmanabhan, "RADAR: An in-building RF-based user location and tracking system," in *Proc. IEEE INFOCOM*, Tel Aviv, Israel, Mar. 2000, vol. 2, pp. 775–784.

[14] B. Sundararaman, U. Buy, and A. Kshemkalyani, "Clock synchronization for wireless sensor networks: A survey," *Ad Hoc Netw.*, vol. 3, no. 3, pp. 281–323, Jan. 2005.

[15] O. Simeone, U. Spagnolini, Y. Bar-Ness, and S. Strogatz, "Distributed synchronization in wireless networks," *IEEE Signal Process. Mag.*, vol. 25, no. 5, pp. 81–97, Sep. 2008.

[16] I. Rhee, J. Lee, J. Kim, E. Serpedin, and Y.-C. Wu, "Clock synchronization in wireless sensor networks: An overview," *Sensors*, vol. 9, pp. 56–85, 2009.

[17] K. Römer and F. Mattern, "Towards a unified view on space and time in sensor networks," *Comput. Commun.*, vol. 28, no. 13, pp. 1484–1497, Aug. 2005.

[18] J. Elson, L. Girod, and D. Estrin, "Fine-grained network time synchronization using reference broadcasts," *SIGOPS Oper. Syst. Rev.*, vol. 36, pp. 147–163, Dec. 2002.

[19] S. Ganeriwal, R. Kumar, and M. B. Srivastava, "Timing-sync protocol for sensor networks," in *Proc. ACM SenSys*, Los Angeles, CA, Nov. 2003, pp. 138–149.

[20] M. Maróti, B. Kusy, G. Simon, and A. Lédeczi, "The flooding time synchronization protocol," in *Proc. ACM SenSys*, Baltimore, MD, Nov. 2004, pp. 39–49.

[21] D. Jeske, "On maximum-likelihood estimation of clock offset," *IEEE Trans. Commun.*, vol. 53, no. 1, pp. 53–54, Jan. 2005.

[22] K.-L. Noh, Q. Chaudhari, E. Serpedin, and B. Suter, "Novel clock phase offset and skew estimation using two-way timing message exchanges for wireless sensor networks," *IEEE Trans. Commun.*, vol. 55, no. 4, pp. 766–777, Apr. 2007.

[23] Q. Chaudhari, E. Serpedin, and K. Qaraqe, "On maximum likelihood estimation of clock offset and skew in networks with exponential delays," *IEEE Trans. Signal Process.*, vol. 56, no. 4, pp. 1685–1697, Apr. 2008.

[24] X. Cheng, A. Thaeler, G. Xue, and D. Chen, "TPS: A time-based positioning scheme for outdoor wireless sensor networks," in *Proc. IEEE INFOCOM*, Hong Kong, China, Mar. 2004, vol. 4, pp. 2685–2696.

[25] H. de Oliveira, E. Nakamura, A. Loureiro, and A. Boukerche, "Localization in time and space for sensor networks," in *Proc. AINA*, Niagara Falls, Ontario, Canada, May 2007, pp. 539–546.

[26] Part 15.4: Wireless Medium Access Control (MAC) and Physical Layer (PHY) Specifications for Low-Rate Wireless Personal Area Networks (WPANs) 2007, IEEE Working Group 802.15.4, Tech. Rep..

[27] B. Denis, J.-B. Pierrot, and C. Abou-Rjeily, "Joint distributed synchronization and positioning in UWB ad hoc networks using TOA," *IEEE Trans. Microw. Theory Tech.*, vol. 54, no. 4, pp. 1896–1911, Jun. 2006.

[28] C. Yan and H. Fan, "Asynchronous self-localization of sensor networks with large clock drift," in *Proc. IEEE MobiQuitous*, Philadelphia, PA, Aug. 2007, pp. 1–8.

[29] K. Yu, Y. Guo, and M. Hedley, "TOA-based distributed localisation with unknown internal delays and clock frequency offsets in wireless sensor networks," *IET Signal Process.*, vol. 3, no. 2, pp. 106–118, 2009.

[30] J. Zheng and Y.-C. Wu, "Joint time synchronization and localization of an unknown node in wireless sensor networks," *IEEE Trans. Signal Process.*, vol. 58, no. 3, pp. 1309–1320, Mar. 2010.

[31] S. Zhu and Z. Ding, "Joint synchronization and localization using TOAs: A linearization based WLS solution," *IEEE J. Sel. Areas Commun.*, vol. 28, no. 7, pp. 1017–1025, Sep. 2010.

[32] Y. Zhou, C. L. Law, Y. L. Guan, and F. Chin, "Indoor elliptical localization based on asynchronous UWB range measurement," *IEEE Trans. Instrum. Meas.*, vol. 60, no. 1, pp. 248–257, Jan. 2011.

[33] A. Perrig, J. Stankovic, and D. Wagner, "Security in wireless sensor networks," *Commun. ACM*, vol. 47, no. 6, pp. 53–57, Jun. 2004.

[34] J. Walters, Z. Liang, W. Shi, and V. Chaudhary, "Wireless sensor networks security: A survey," *Security in Distributed, Grid, Pervasive Comput.*, pp. 367–405, 2007.

[35] M. Flury, M. Poturalski, P. Papadimitratos, J.-P. Hubaux, and J.-Y. Le Boudec, "Effectiveness of distance-decreasing attacks against impulse radio ranging," in *Proc. ACM WiSec*, Hoboken, NJ, Mar. 2010, pp. 117–128.

[36] L. Lazos and R. Poovendran, "SeRLoc: Secure range-independent localization for wireless sensor networks," in *Proc. ACM WiSe*, Philadelphia, PA, Oct. 2004, pp. 21–30.

[37] S. Capkun and J.-P. Hubaux, "Secure positioning of wireless devices with application to sensor networks," in *Proc. IEEE INFOCOM*, Miami, FL, Mar. 2005, vol. 3, pp. 1917–1928.

[38] Y. Chen, W. Trappe, and R. P. Matrin, "Attack detection in wireless localization," in *Proc. IEEE INFOCOM*, Anchorage, AK, May 2007, pp. 1964–1972.

[39] Z. Li, W. Trappe, Y. Zhang, and B. Nath, "Robust statistical methods for securing wireless localization in sensor networks," in *Proc. IPSN*, Los Angeles, CA, Apr. 2005, pp. 91–98.

[40] D. Liu, P. Ning, A. Liu, C. Wang, and W. K. Du, "Attack-resistant location estimation in wireless sensor networks," *ACM Trans. Inf. Syst. Secur.*, vol. 11, no. 4, pp. 1–39, Jul. 2008.

[41] Z. Sahinoglu and S. Gezici, "Ranging in the IEEE 802.15.4a standard," in *Proc. IEEE WAMICON*, Clearwater, FL, Dec. 2006, pp. 1–5.

[42] B. Denis and N. Daniele, "NLOS ranging error mitigation in a distributed positioning algorithm for indoor UWB ad-hoc networks," in *Proc. IEEE IWWAN*, Oulu, Finland, May 2004, pp. 356–360.

[43] H. Kopetz and W. Ochsenreiter, "Clock synchronization in distributed real-time systems," *IEEE Trans. Commun.*, vol. C-36, no. 8, pp. 933–940, Aug. 1987.

[44] Y. Wang, X. Ma, and G. Leus, "An UWB ranging-based localization strategy with internal attack immunity," in *Proc. IEEE ICUWB*, Nanjing, China, Sep. 2010, pp. 1–4.

[45] Z. Sahinoglu and S. Gezici, "Enhanced position estimation via node cooperation," in *Proc. IEEE ICC*, Cape Town, South Africa, May 2010, pp. 1–6.

[46] P. Stoica and J. Li, "Lecture notes—source localization from range-difference measurements," *IEEE Signal Process. Mag.*, vol. 23, no. 6, pp. 63–66, Nov. 2006.

[47] Y. Wang, G. Leus, and X. Ma, "Time-based localization for asynchronous wireless sensor networks," in *Proc. IEEE ICASSP*, Prague, Czech Republic, May 2011, pp. 3284–3287.

[48] G. J. Pottie and W. J. Kaiser, "Wireless integrated network sensors," *Commun. ACM*, vol. 43, no. 5, pp. 51–58, May 2000.

Yiyin Wang (S'07) received the B.S. degree in electrical engineering from Fudan University, Shanghai, China, in 2002, and the M.S. degree (*cum laude*) in microelectonics from the Delft University of Technology, The Netherlands, and Fudan University, Shanghai, China, in 2005, respectively.

From 2005 to 2006, she was a Research Assistant with ASIC and System State Key Lab, Fudan University. From 2006 to 2007, she was a Research Assistant with the Circuits and Systems group (CAS), Faculty of Electrical Engineering, Mathematics and Computer Science (EEMCS), Delft University of Technology, The Netherlands. Since November 2007, she has been a Ph.D. degree candidate in the same group.

From February 2010 until July 2010, she was a Visiting Student with the Georgia Institute of Technology, Atlanta. Her research interests include signal processing for tracking, localization and communications based on ultrawideband technologies.

Xiaoli Ma (M'03–SM'09) received the B.S. degree in automatic control from Tsinghua University, Beijing, China in 1998, the M.S. degree in electrical engineering from the University of Virginia, Blacksburg, in 2000, and the Ph.D. degree in electrical engineering from the University of Minnesota, Minneapolis, in 2003.

From 2003 to 2005, she was an Assistant Professor of Electrical and Computer Engineering, Auburn University. Since 2006, she has been with the School of Electrical and Computer Engineering, Georgia Institute of Technology, Atlanta, where she is currently an Associate Professor. Her research interests include transceiver designs and diversity techniques for wireless fading channels, channel modeling, estimation and equalization, carrier frequency synchronization for OFDM systems, routing, and cooperative designs for wireless networks.

Geert Leus (M'00–SM'05) was born in Leuven, Belgium, in 1973. He received the electrical engineering degree and the Ph.D. degree in applied sciences from the Katholieke Universiteit Leuven, Belgium, in June 1996 and May 2000, respectively.

He has been a Research Assistant and a Postdoctoral Fellow of the Fund for Scientific Research—Flanders, Belgium, from October 1996 to September 2003. During that period, he was affiliated with the Electrical Engineering Department, Katholieke Universiteit Leuven, Belgium. Currently, he is an Associate Professor with the Faculty of Electrical Engineering, Mathematics and Computer Science, Delft University of Technology, The Netherlands. During summer 1998, he visited Stanford University, Stanford, CA, and from March 2001 to May 2002, he was a Visiting Researcher and Lecturer with the University of Minnesota, Minneaplois. His research interests are in the area of signal processing for communications.

Dr. Leus received a 2002 IEEE Signal Processing Society Young Author Best Paper Award and a 2005 IEEE Signal Processing Society Best Paper Award. He was the Chair of the IEEE Signal Processing for Communications and Networking Technical Committee, and an Associate Editor for the IEEE TRANSACTIONS ON SIGNAL PROCESSING, the IEEE TRANSACTIONS ON WIRELESS COMMUNICATIONS, and the IEEE SIGNAL PROCESSING LETTERS. Currently, he serves on the Editorial Board of the EURASIP *Journal on Applied Signal Processing*.